Movement and Crevices Around a Sodium Channel S3 Segment

Thao P. Nguyen[1,2] and Richard Horn[1]

[1]Department of Physiology, Jefferson Medical College, Philadelphia, PA 19107; [2]Institute of Neurological Sciences, University of Pennsylvania, Philadelphia, PA 19104

ABSTRACT Voltage sensing is due mainly to the movement of positively charged S4 segments through the membrane electric field during changes of membrane potential. The roles of other transmembrane segments are under study. The S3 segment of domain 4 (D4/S3) in the sodium channel $Na_v1.4$ carries two negatively charged residues and has been implicated in voltage-dependent gating. We substituted cysteines into nine putative "high impact" sites along the complete length of D4/S3 and evaluated their accessibilities to extracellular sulfhydryl reagents. Only the four outermost substituted cysteines (L1433C, L1431C, G1430C, and S1427C) are accessible to extracellular sulfhydryl reagents. We measured the voltage-dependent modification rates of the two cysteines situated at the extreme ends of this accessible region, L1433C and S1427C. Independent of the charge on the sulfhydryl reagents, depolarization increases the reactivity of both of these residues. Thus, the direction of the voltage dependence is opposite to that expected for a negatively charged voltage sensor, namely an inward translational movement in response to depolarization. Intrinsic electrostatic potentials were probed by charged sulfhydryl reagents and were either negative or positive, respectively, near L1433C and S1427C. The magnitude of the electrostatic potential near S1427C decreases with depolarization, suggesting that the extracellular crevice next to it widens during depolarization. S1427C experiences 44% of the electric field, as probed by charged cysteine reagents. To further explore movements around D4/S3, we labeled cysteines with the photoactivatable cross-linking reagent benzophenone-4-carboxamidocysteine methanethiosulfonate and examined the effects of UV irradiation on channel gating. After labeling with this reagent, all accessible cysteine mutants show altered gating upon brief UV irradiation. In each case, the apparent insertion efficiency of the photoactivated benzophenone increases with depolarization, indicating voltage-dependent movement near the extracellular end of D4/S3.

KEY WORDS: cysteine accessibility • photocross-linking • benzophenone • voltage-dependent movement • electrostatic potential

INTRODUCTION

Voltage-gated ion channels depend on positively charged S4 segments to sense and respond to changes in membrane potential (Sigworth, 1994; Bezanilla, 2000). Other transmembrane segments (S1–S3, S5, S6) are typically devoid of basic residues, except for a single positively charged residue near the cytoplasmic end of S2 segments. However, the S1 segments of sodium channels, especially in the second, third, and fourth homologous domains, contain one or two conserved acidic residues (Keynes and Elinder, 1999). Moreover, S2 and S3 segments contain highly conserved acidic residues, either glutamate or aspartate (Keynes and Elinder, 1999; Bezanilla, 2000). S2 or S3 segments could, therefore, act as voltage sensors if these negatively charged residues move through the electric field during changes of membrane potential. These acidic residues may also be involved in electrostatic interactions with positively charged S4 residues (Papazian et al., 1995; Planells-Cases et al., 1995; Seoh et al., 1996; Tiwari-Woodruff et al., 1997, 2000; Cha and Bezanilla, 1997.

Address correspondence to Dr. Richard Horn, Department of Physiology, Jefferson Medical College, 1020 Locust St., Philadelphia, PA 19107. Fax: (215) 503-2073; E-mail: Richard.Horn@TJU.edu

Previous work from this laboratory has shown that in response to depolarization, the S4 segment of domain 4 (D4/S4) of the human skeletal muscle sodium channel ($hNa_V1.4$) translocates its three most external positive charges from a buried or intracellular position into a large, negatively charged hydrophilic vestibule on the extracellular surface of the channel (Yang and Horn, 1995; Yang et al., 1996, 1997).

Of the three transmembrane segments with acidic residues, S3 holds particular interest, structurally and functionally. Structurally, whereas S1 and S2 appear to be simple amphipathic α-helices interfacing directly with lipid and protein on opposite faces, the secondary structure and the surrounds of S3 present a more complicated picture, based on scanning mutagenesis studies (Monks et al., 1999; Hong and Miller, 2000; Li-Smerin et al., 2000; Li-Smerin and Swartz, 2001). The S3 segment in the *drk1* potassium channel, for example, has been depicted as internal and external helices, surrounded by different environments, playing different roles, and separated by a proline kink (Li-Smerin and Swartz, 2001).

Functionally, neutralization of a conserved aspartate in the S3 segment of potassium channels has profound effects on activation gating (Papazian et al., 1995;

Planells-Cases et al., 1995; Seoh et al., 1996; Hong and Miller, 2000; Li-Smerin et al., 2000). The extracellular end of the S3 segment also contributes to the binding site for toxins that modify gating of potassium channels (Li-Smerin and Swartz, 2000). In sodium channels, an inherited disorder of skeletal muscles that causes episodic myotonia in horses is due to a point mutation in the S3 segment of domain 4 (D4/S3; Cannon et al., 1995). Moreover, a point mutation (L1433R) in the D4/S3 segment of the human skeletal muscle sodium channel $Na_v1.4$ has been linked genetically with the disease paramyotonia congenita (Ptacek et al., 1993). Subsequent studies, examining point mutations of L1433 in heterologously expressed channels, confirmed a role in gating (Yang et al., 1994; Ji et al., 1996). It has furthermore been suggested that D4/S3 might interact with the voltage sensor D4/S4 during activation and recovery from inactivation (Ji et al., 1996).

The purpose of this study is to explore the roles played by D4/S3 in voltage-dependent gating. To this end, we used two approaches. First, we evaluated the accessibilities of nine individually substituted cysteines along the full length of D4/S3. These "high impact" residues were chosen by homology with potassium channel residues that are believed to be involved in protein–protein interactions between S3 and other transmembrane segments (Hong and Miller, 2000; Li-Smerin et al., 2000). For two of these mutants, L1433C and S1427C, we tested whether cysteine modification rates depended on membrane potential. Second, we examined the biophysical consequences of immobilizing D4/S3 using a cysteine-reactive photocross-linking reagent.

Our results show that the high impact residues of D4/S3 line a narrow extracellular crevice that reaches down to the putative kink. This crevice appears to widen in response to depolarization. Photocross-linking results argue for voltage-dependent movement near the external end of D4/S3.

MATERIALS AND METHODS

Molecular Biology

Cysteine mutants were generated by QuickChange site-directed mutagenesis (Stratagene) and inserted into the mammalian expression construct pRcCMV- or pCDNA1-h$Na_v1.4$. The cysteine mutant of L1433 is a gift from Dr. A.L. George (Vanderbilt University, Nashville, TN). The tsA201 cells were transiently transfected using a standard calcium phosphate method (Margolskee et al., 1993). Positively transfected cells were identified by decoration with CD8 antibody-coated beads, using coexpressed CD8 (Jurman et al., 1994).

Electrophysiology

Standard whole-cell recording methods were used. The patch pipette solution contained (in mM) 105 CsF, 35 NaCl, 10 EGTA, 10 Hepes; pH 7.4 titrated with CsOH. The bath solution, also used for perfusion, contained (in mM) 150 NaCl, 2 KCl, 1.5 $CaCl_2$, 1 $MgCl_2$, 10 Hepes; pH 7.4 titrated with CsOH. Cells expressed large sodium currents (>2 nA at −25 mV) 1–3 d after transfection. Corrections were made for liquid junction potentials. Series resistance was <3 MΩ and voltage error <3 mV after compensation. Data were filtered at 5–10 kHz and acquired with Clampex 8.2 (Axon Instruments, Inc.). Experiments were performed at room temperature (~22°C).

In the substituted cysteine accessibility experiments, the negatively charged methanethiosulfonate ethylsufonate (MTSES),* the negatively charged benzophenone-4-carboxamidocysteine methanethiosulfonate (BPMTS), or the positively charged methanethiosulfonate ethyltrimethylammonium (MTSET) was applied in the extracellular bath solutions. These reagents are all membrane impermeant. Concentrated aqueous (for MTSES and MTSET) or ethyl acetate (for BPMTS) stocks of these reagents were stored at 4°C up to 1 wk and diluted in bath or perfusion solutions immediately before use. In experiments characterizing the biophysical consequences of cysteine modification, all the cells in a 35-mm dish were exposed to high concentrations of an MTS reagent added to the bath solution; the cells were then washed twice with bath solution before recording. Exposure time was 10 min for MTSES (5 mM), 15 min for BPMTS (1 mM), and 20 min for MTSET (2–5 mM). For MTSET, because of its short lifetime at neutral pH (see below), the reagent solution was refreshed after the first 10 min of exposure. The high concentrations and long exposure times were designed to ensure maximum labeling. Moreover, subsequent experiments showed weak voltage dependence of modification, indicating that the resting potential of the cells was not a concern.

In experiments measuring cysteine modification rate, reagent-free and reagent-containing solutions were perfused onto single patch-clamped cells using borosilicate theta tubes with inner tip-diameters of 50–100 μm per lumen, regulated by a computer-controlled rapid solution switching system (LSS-3200; Burleigh Instruments, Inc.). The voltage step used to drive the piezo motor was lowpass filtered at 60 Hz to smooth the movement of the theta tube. For these experiments, the cells were raised from the dish during whole cell recording and presented to the theta tube. Solutions were delivered at 170–300 μl/min. In control experiments the speed of solution exchange at the cell was determined by measuring the rate of change of sodium current amplitude in response to a change in extracellular sodium concentration, using sodium channels mutated to remove fast inactivation (Vedantham and Cannon, 1998). The time constant for solution exchange was <4 ms after a constant motor delay of <15 ms. Therefore, in designing protocols for reagent application we assumed that solution change was complete after 30 ms. Bath volume was maintained throughout the experiment by continuous aspiration.

In the photocross-linking experiments, the photoactivable cross-linker BPMTS was used (Horn et al., 2000). To label cysteines, BPMTS was applied for 15 min onto cells attached to a coverslip, then washed away. The coverslip was used as the bottom of a recording chamber. To photoactivate benzophenone, UV light was directed to a voltage-clamped BPMTS-prelabeled cell through a 40× (1.3 N.A.) oil immersion objective (S Fluor; Nikon). The UV light source was a continuously operating 75-W xenon arc lamp interrupted by a mechanical shutter (IonOptix). Light was bandpass filtered between 340–380 nm to reduce photodamage and heat.

**Abbreviations used in this paper:* BPMTS, benzophenone-4-carboxamidocysteine methanethiosulfonate; MTSES, methanethiosulfonate ethylsulfonate; MTSET, methanethiosulfonate ethyltrimethylammonium.

Data Analysis

Data were analyzed using Clampfit 8.2 (Axon instruments, Inc.) and Origin 6.1 (Microcal Software, Inc.). Results are tabulated as mean ± SEM.

Standard Fits of Voltage Dependence and Kinetics of Gating

Steady-state activation (G-V) and inactivation (h_∞) curves were obtained by fitting normalized peak currents G/G_{max} and I/I_{max}, respectively, with single Boltzmann functions,

$$\frac{1}{1+\exp\left(\frac{\delta F(V_{0.5}-V)}{RT}\right)},$$

where V is the membrane potential, $V_{0.5}$ the half-activation or half-inactivation voltage, δ the apparent gating charge, F Faraday's constant, R the universal gas constant, and T the temperature in Kelvin, with $RT/F = 25$ mV at 22°C. Inactivation time constants (τ_h) were derived from fitting the inactivation phase of current traces with an exponential decay of first order, unless otherwise indicated. Time constants of recovery from fast inactivation (τ_{rcv}) were also obtained from first order relaxations (O'Leary et al., 1995). To obtain the apparent gating charge δ_{rec} associated with the recovery from inactivation, τ_{rcv} values at different recovery potentials were fit by a single exponential growth function, $\tau_{rev}(V) = \tau_{rev}(0) \times \exp(\delta_{rec} FV/RT)$.

Cysteine Modification

Second order rate constants (k_{mod}) for cysteine modification at different membrane potentials were obtained using variations of methods previously developed in this laboratory (Yang and Horn, 1995; Mitrovic et al., 1998). Specifically, modification of the D4/S3 mutant L1433C by either MTSET or MTSES causes a slowing of inactivation. This was tracked by measuring the time course of an isochronal increase in sodium current at a test potential of −30 mV. The time point for this measurement, determined *a posteriori* for each cell, was that which maximized the effect of cysteine modification on the amplitude of current increase. Modification of S1427C, by contrast, causes a hyperpolarizing shift of steady-state inactivation. This was measured from the relative decrease in peak current at −25 mV, before and after a 100-ms prepulse to −90 mV from a holding potential of −150 mV. MTSET and MTSES were applied at −150, 0, or a positive potential (either 40 or 50 mV), using the fast perfusion system described earlier. At −150 mV the cells were exposed to reagent for 10 or 20 s between test sweeps to assess degree of modification. At the more positive potentials, the exposures were 10 s each, followed by at least 10 s at −150 mV in the absence of reagent to allow for full recovery from inactivation. Because we used 10-s depolarizations during cysteine modification, the channels were likely to be inactivated. Therefore, any voltage dependence of modification could be due to conformational differences between resting closed channels and inactivated channels.

For MTSES, the time course of modification was fit by a first order exponential decay, yielding a pseudo-first order rate constant that, when divided by MTSES concentration ([MTSES]), gives an estimate of k_{mod}. Our estimates of k_{mod} for MTSET take into account the short half-life of this reagent, a consequence of hydrolysis in a buffered aqueous solution at neutral pH ($t_{1/2} = 11.2$ min; Karlin and Akabas, 1998). The exponential decrease in [MTSET] has a rate $k_{hyd} = -\ln(0.5)/t_{1/2} = 1.03 \times 10^{-3}\ s^{-1}$. Because of the rapidity of this reaction, the observed time course of modification, which is typically first order when the reagent concentration is fixed (Karlin and Akabas, 1998; Horn, 1998), may be influenced by the decay of [MTSET]. For example, if modification is measured over a 5-min period, [MTSET] will decrease by >26%, which does not take into account the time required, on the order of ~3 min, to load the freshly prepared solution into the perfusion tubing and position it for application to a cell. If MTSET is applied to an exposed cysteine residue at an initial concentration M_0, the time course of irreversible modification $S_{mod}(t)$ will be given by

$$S_{mod}(t) = 1 - \exp\left(-k_{mod} M_0 \int_0^t e^{-u \cdot k_{hyd}}\, du\right)$$

$$= 1 - \exp\left[-\frac{k_{mod}}{k_{hyd}} M_0 (1 - e^{-t \cdot k_{hyd}})\right].$$

Appropriately,

$$\lim_{k_{hyd} \to 0} S_{mod}(t) = 1 - \exp(-k_{mod} M_0 t).$$

This theoretical relationship must be modified to account for the fact that we applied reagents repetitively, rather than continuously. During exposures of up to 20 s, [MTSET] decays ~2%, an amount we assumed to be negligible for each exposure. However, [MTSET] is expected to decay during the course of successive exposures. Therefore, for each presentation of reagent, we calculated the expected [MTSET], based on the aforementioned value of k_{hyd} and the elapsed time after diluting the stock solution of reagent into our buffered perfusion solution. The biophysical effect of each exposure was then plotted against the cumulative product of the exposure times and the calculated [MTSET]. The course of the reaction was fit by a decaying exponential function with eigenvalue k_{mod}.

Electrostatic Potentials

The electrostatic potential Ψ_V in the vicinity of an introduced cysteine at membrane potential V can be estimated if the relative reactivity of that residue to MTSET and MTSES ($v_{Cys} = \frac{k_{mod,MTSET,V}}{k_{mod,MTSES,V}}$) is compared with that of a free thiol (e.g., β-mercaptoethanol), using a "ratio-of-ratios" method (Stauffer and Karlin, 1994; Pascual and Karlin, 1998). The relative reactivity of β-mercaptoethanol to MTSET and MTSES, $v_{\beta ME}$, is 12.5 (Karlin and Akabas, 1998). Hence, for an introduced cysteine in the sodium channel, the ratio-of-ratios is $\rho_V = \left(\frac{k_{mod,MTSET,V}}{k_{mod,MTSES,V}}\right)/12$, where $k_{mod,MTS,V}$ is the measured second order rate constant for the modification of that cysteine by an MTS reagent at voltage V.

The ratio-of-ratios method factors out the inherent reactivity of a given cysteine residue, including its ionization state (Stauffer and Karlin, 1994; Pascual and Karlin, 1998). The electrostatic potential Ψ_V is the sum of an intrinsic electrostatic potential $\Psi_{i,V}$ and the fraction δ_{cys} of the extrinsic membrane potential V near the cysteine residue, expressed as $\Psi_V = \Psi_{i,V} + \delta_{cys} V$ (Yang et al., 1997; Pascual and Karlin, 1998). The relationship between relative cysteine reactivity ρ_V and Ψ_V is given by

$$\rho_V = \exp\left(\frac{-(z_{MTSET} - z_{MTSES}) F \Psi_V}{RT}\right) = \exp\left(\frac{-2F(\Psi_{i,V} + \delta_{cys} V)}{RT}\right), \quad (1)$$

where the valences of the reagents are $z_{MTSET} = 1$ and $z_{MTSES} = -1$ (Pascual and Karlin, 1998).

Eq. 1 has two unknowns, $\Psi_{i,V}$ and δ_{cys}. However, the intrinsic electrostatic potential $\Psi_{i,V}$ can be determined uniquely at $V = 0$ mV, using Eq. 1 and the measured value of ρ_V. Rearranging,

$$\Psi_{i,0} = -\frac{RT}{2F} \ln(\rho_0). \quad (2)$$

Note that Eq. 2 can be generalized to all membrane potentials if $\delta_{cys} = 0$, as has been observed for specific substituted cysteines in

previous studies (Yang et al., 1997; Elinder et al., 2001). We will show in this study that $\delta_{cys} > 0$ for at least one cysteine residue in D4/S3.

In general, $\Psi_{i,V}$ depends on membrane potential, because changes of membrane potential produce conformational changes that may alter the local electrostatic environment near a cysteine residue. However, because the steady-state effects of membrane potential on channel gating have saturated by voltages as positive as 0 mV for all of our cysteine mutants (Fig. 2, and Mitrovic et al., 2000), we assume that $\Psi_{i,V}$ is independent of membrane potential for $V \geq 0$ mV. In this case we can estimate δ_{cys} by

$$\delta_{Cys} = \frac{RT}{2FV} \ln(\rho_0/\rho_V),\ V \geq 0 \text{ mV}. \quad (3)$$

Note that this estimate of δ_{cys} strictly applies to nonnegative membrane potentials. Conformational changes at more negative membrane potentials might change the dielectric environment of a crevice in which a cysteine resides. This could change the shape of the electric field, and therefore the location of the cysteine residue within the electric field. For this reason, we present estimates of $\Psi_{i,V}$ at negative potentials using the full range of possible values of δ_{cys} from 0 to 1 (Fig. 9).

RESULTS

Perturbation of Channel Gating by Cysteine Substitutions

A "high impact" face of S3 segments of potassium channels has been identified by the relative biophysical consequences of mutating individual S3 residues (Hong and Miller, 2000; Li-Smerin et al., 2000; Li-Smerin and Swartz, 2001). High impact residues are postulated to occur where significant protein–protein interactions are altered by changes in membrane potential. Fig. 1 A shows an alignment of the S3 segments of two potassium channels with the S3 segment of the fourth domain of the human skeletal sodium channel α subunit. High impact residues are underlined and bolded. The helical net display of D4/S3 (Fig. 1 B) shows that high impact residues would lie mainly along one face of an α helix. Fig. 1 A highlights two well-conserved features of S3 segments, a negatively charged aspartate residue closer to the intracellular end of S3, and a region proposed to act as a kink between two α helices (Li-Smerin and Swartz, 2001). A proline residue in potassium channels and a serine residue in D4/S3 of sodium channels were suggested to be pivot points in this kink, based in part on an analysis of known protein structures (Li-Smerin and Swartz, 2001).

We engineered nine individual cysteine substitutions along the full length of D4/S3, selecting only the putative high impact residues, including both the conserved aspartate D1420 and the serine S1427 at the postulated kink (Fig. 1 A). Sodium channel gating was assessed from whole cell currents in tsA201 cells transiently

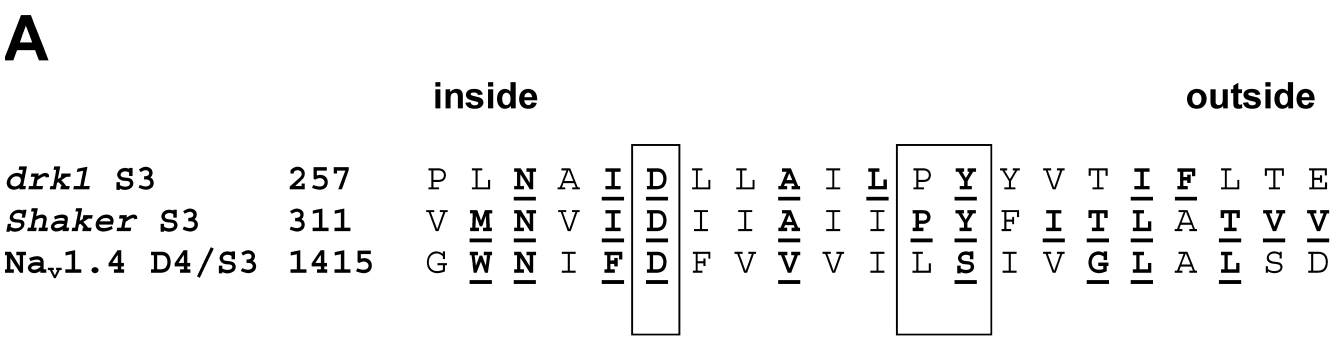

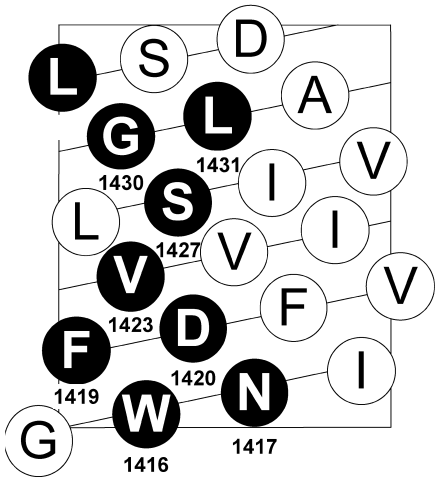

FIGURE 1. (A) Sequence alignment of D4/S3 of the human skeletal muscle sodium channel Nav1.4 with S3 segments of *Shaker* and *drk1* potassium channels. High impact residues in S3 of potassium channels and cysteine mutants in D4/S3 of sodium channel are underlined and bolded. The nine D4/S3 mutations are W1416C, N1417C, F1419C, D1420C, V1423C, S1427C, G1430C, L1431C, and L1433C. G1430 is also aligned with T268 in the brain mKv1.1 potassium channel (sequence not shown), which is also implicated in a role in gating (Planells-Cases et al., 1995). F1419 is aligned with a disease-associated phenylalanine residue in D4/S3 of the equine isoform of $Na_V1.4$ (Cannon et al., 1995). Numbers indicate residue positions starting from the inside. The large box highlights the short kink postulated to separate the two helices (Li-Smerin and Swartz, 2001). The small box highlights the conserved Asp in S3. (B) α-helical net of D4/S3 in the human skeletal muscle sodium channel $Na_v1.4$. The residues substituted to cysteines in this study are shown in black circles.

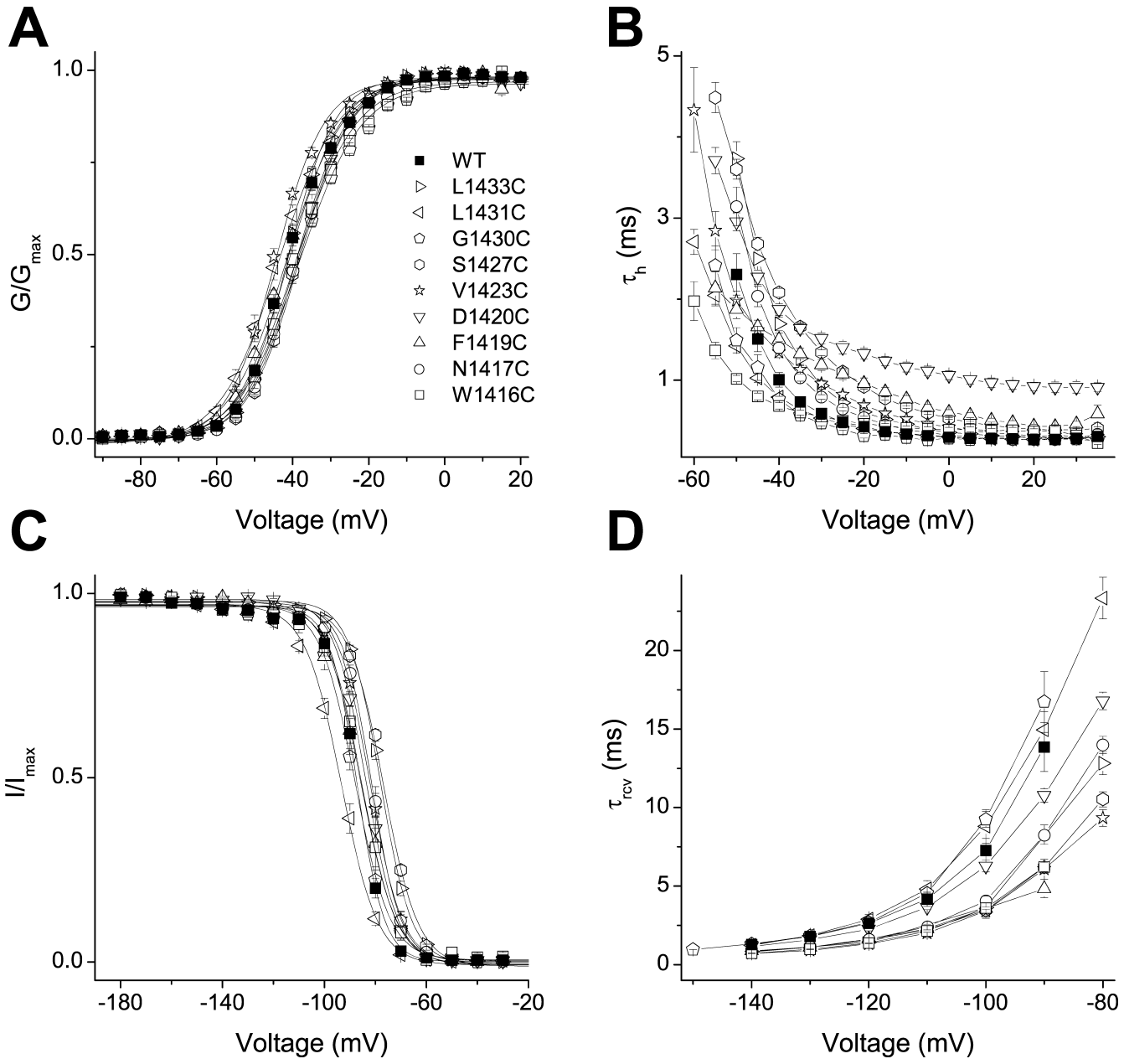

FIGURE 2. Perturbations in channel gating by cysteine mutations of the putative "high impact" face of Nav1.4 D4/S3. (A) Voltage-activation relations. Currents were elicited from a holding voltage of −140 mV to voltages between −55 and 65 mV in 5-mV increments. Symbols represent normalized whole cell conductances, obtained by dividing peak currents by the driving force. Solid curves are averages of single Boltzmann fits of normalized conductances from individual cells. (B) Fast inactivation. Inactivation time constants (τ_h) were obtained from fitting the current decay during depolarization measured in Fig. 2 A. A single exponential relaxation was performed for WT and most mutants; a double exponential relaxation for L1433C and G1430C. Only data in the range from −60 to 35 mV are shown. (C) Steady-state inactivation. Inactivation was induced from a holding voltage of −150 mV by a 100-ms conditioning pulse to a voltage between −180 and −30 mV in 10-mV increments. Solid curves are averages of single Boltzmann fits of normalized currents at a test pulse −25 mV from individual cells. (D) Recovery from fast inactivation. A triple pulse protocol, with a holding voltage of −140 mV and test pulses to −25 mV, was used to measure recovery from inactivation at different recovery potentials between −140 and −80 mV in 10-mV increments (or between −150 and −90 mV for G1430C). Recovery time constants (τ_{rcv}) were obtained from single exponential fits. Data and typical parameters derived from fits are listed in Table I. For all panels, $n \geq 3$.

transfected with wild type or mutated DNA encoding these sodium channel α subunits. All mutants were tolerant of cysteine substitution, producing functional channels with only mildly perturbed gating (Fig. 2, Table I). Among all the mutants, G-V curves derived from peak currents showed shifts of $V_{0.5}$ of <4 mV. The shifts were somewhat larger for steady-state inactivation, the largest being a 10.4-mV depolarizing shift for S1427C.

TABLE I

Effects of Extracellular MTSES on the Gating of Wild-type and Mutant D4/S3 Nav1.4 Channels

	G-V			Inactivation	
	$V_{0.5}$	δ	*n*	$\tau_{h,\ -40\ mV}$	*n*
	mV			*ms*	
WT	−40.9 ± 0.6	3.67 ± 0.13	7	1.01 ± 0.09	7
$MTSES_{ext}$	−39.2 ± 0.7	3.35 ± 0.15	7	0.92 ± 0.05	8
L1433C	−41.2 ± 0.6	4.10 ± 0.09	14	1.69 ± 0.08	14
$MTSES_{ext}$	−41.8 ± 0.8	4.15 ± 0.15	8	3.85 ± 0.11[b]	8
L1431C	−43.6 ± 1.1	3.26 ± 0.06	14	0.79 ± 0.04	14
$MTSES_{ext}$	−42.3 ± 1.8	3.43 ± 0.26	8	0.70 ± 0.05	8
G1430C	−38.3 ± 0.6	3.11 ± 0.05	6	0.76 ± 0.04	6
$MTSES_{ext}$	−43.3 ± 1.9[a]	3.21 ± 0.06	6	1.01 ± 0.04[b]	6
S1427C	−38.1 ± 0.6	3.72 ± 0.04	25	2.08 ± 0.05	25
$MTSES_{ext}$	−44.0 ± 1.3[b]	3.11 ± 0.09[b]	7	1.13 ± 0.05[b]	7
V1423C	−44.5 ± 0.6	3.92 ± 0.13	4	1.35 ± 0.07	5
$MTSES_{ext}$	−44.8 ± 0.3	3.74 ± 0.22	5	1.52 ± 0.09	5
D1420C	−38.9 ± 0.9	3.68 ± 0.14	7	1.87 ± 0.07	7
$MTSES_{ext}$	−40.8 ± 0.9	3.64 ± 0.06	5	1.82 ± 0.11	5
F1419C	−41.6 ± 0.3	3.41 ± 0.21	4	1.50 ± 0.08	6
$MTSES_{ext}$	−43.5 ± 0.9	3.55 ± 0.23	4	1.50 ± 0.08	4
N1417C	−38.1 ± 0.9	3.65 ± 0.06	12	1.40 ± 0.07	12
$MTSES_{ext}$	−36.9 ± 0.8	3.45 ± 0.10	6	1.49 ± 0.10	6
W1416C	−39.2 ± 0.7	3.20 ± 0.13	4	0.80 ± 0.04	4
$MTSES_{ext}$	−39.3 ± 1.3	3.04 ± 0.10	3	0.93 ± 0.05	3

	Steady-state inactivation			Recovery from fast inactivation		
	$V_{0.5}$	δ	*n*	$\tau_{rev,\ -100\ mV}$	δ	*n*
	mV			*ms*		
WT	−87.2 ± 0.9	4.70 ± 0.15	7	7.27 ± 0.77	1.70 ± 0.12	4
$MTSES_{ext}$	−88.9 ± 0.8	4.25 ± 0.17	7	8.63 ± 0.82	1.45 ± 0.17	6
L1433C	−78.0 ± 0.6	4.09 ± 0.11	13	3.63 ± 0.21	1.76 ± 0.04	4
$MTSES_{ext}$	−69.3 ± 0.9[b]	3.28 ± 0.05[b]	10	2.06 ± 0.11[b]	1.38 ± 0.04[b]	3
L1431C	−93.3 ± 1.1	3.55 ± 0.10	13	8.81 ± 1.06	1.15 ± 0.12	5
$MTSES_{ext}$	−102.4 ± 1.0[b]	4.27 ± 0.13[b]	8	36.63 ± 1.03[b]	1.57 ± 0.10[a]	4
G1430C	−88.0 ± 1.0	3.73 ± 0.24	5	9.25 ± 0.49	1.95 ± 0.15	3
$MTSES_{ext}$	−95.9 ± 1.1[b]	3.07 ± 0.06[a]	6	6.49 ± 0.08[a]	1.04 ± 0.11[b]	4
S1427C	−76.8 ± 0.4	3.75 ± 0.09	25	3.47 ± 0.17	1.51 ± 0.05	10
$MTSES_{ext}$	−100.9 ± 1.5[b]	2.70 ± 0.07[b]	7	4.41 ± 0.22[b]	ND	7
V1423C	−82.2 ± 1.0	3.99 ± 0.13	6	3.42 ± 0.47	1.31 ± 0.17	5
$MTSES_{ext}$	−82.7 ± 1.4	3.76 ± 0.04	4	4.32 ± 0.34	1.13 ± 0.14	5
D1420C	−83.6 ± 0.8	3.95 ± 0.04	7	6.27 ± 0.38	1.25 ± 0.08	5
$MTSES_{ext}$	−85.7 ± 1.0	4.04 ± 0.10	5	7.29 ± 0.66	1.04 ± 0.15	3
F1419C	−85.6 ± 2.4	3.59 ± 0.10	6	3.58 ± 0.53	0.94 ± 0.10	4
$MTSES_{ext}$	−87.0 ± 1.1	3.61 ± 0.11	5	3.98 ± 0.22	1.13 ± 0.09	4
N1417C	−81.5 ± 0.9	4.45 ± 0.10	12	4.06 ± 0.30	1.76 ± 0.06	7
$MTSES_{ext}$	−80.6 ± 1.3	4.72 ± 0.12	6	4.43 ± 0.57	1.68 ± 0.17	5
W1416C	−85.4 ± 1.4	3.78 ± 0.14	5	3.59 ± 0.08	1.53 ± 0.05	4
$MTSES_{ext}$	−88.1 ± 2.1	3.85 ± 0.24	3	4.28 ± 0.45	1.19 ± 0.29	3

The values of τ_h for most cases were derived from single-order exponential fits, except for L1433C without reagent and G1430C ± MTSES. For these three cases, second-order exponential fits were required and the more heavily weighted component (usually the faster component) of the two resulting time constants was shown. τ_{rcv} values were assessed for most cases in the range of potentials from −140 to −80 mV in 10-mV (or 20-mV for L1433C) increments. Exceptionally, for L1431C mV + MTSES, the recovery relationship was so drastically shifted towards a more hyperpolarized direction that recovery at potentials from −160 to −100 mV was assessed instead. Similarly, for G1430C ± MTSES, the recovery relations revealed a much smaller hyperpolarizing shift; therefore, τ_{rcv} values were measured in the range of −150 to −90 mV. To obtain the δ value associated with recovery, τ_{rcv} values at different recovery potentials were fit to a single exponential growth. One noted exception is S1427C + MTSES, where an exponential growth fit could not be performed due to the loss of voltage dependence. Data are presented as mean ± SEM (*n*). $V_{0.5}$, half-activation or half-inactivation voltage, derived from single Boltzmann fits to individual GV relations or h_∞ curves, respectively; δ, apparent gating charge; $\tau_{h,\ -40\ mV}$, time constant of fast inactivation at −40 mV; $\tau_{rcv,\ -100\ mV}$, time constant of recovery from fast inactivation at −100 mV.

[a]$P < 0.05$.

[b]$P < 0.01$.

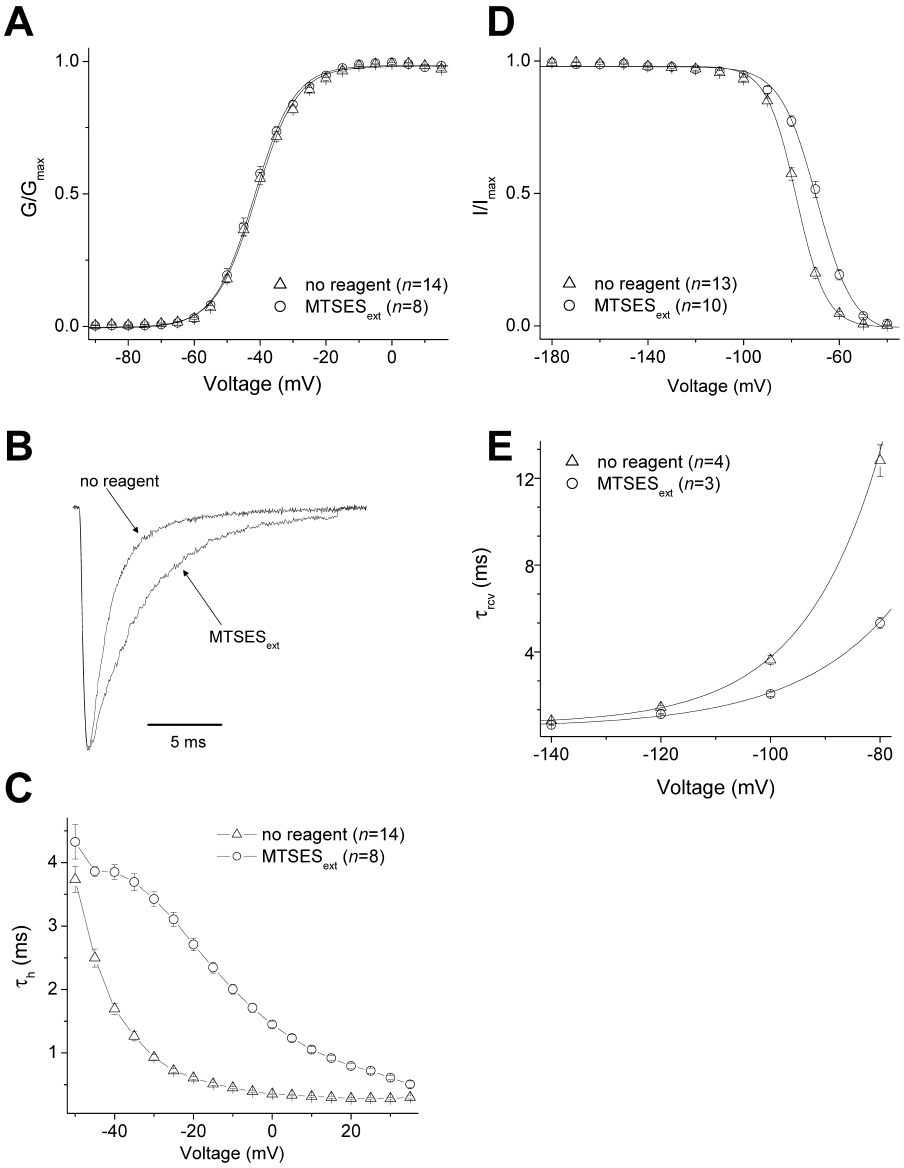

FIGURE 3. Effects of external MTSES on the gating properties of L1433C. Protocols were as described in Fig. 2. (A) Voltage-activation relations. (B) Scaled currents were activated by a depolarization from −140 to −40 mV. (C) Fast inactivation. While a single exponential fit was adequate to derive τ_h values for the "$MTSES_{ext}$" condition, a double exponential fit was required for the "no reagent" condition and the more heavily weighted component was plotted. (D) Steady-state inactivation. (E) Recovery from fast inactivation. Solid curves are averages of single exponential growth fits of the τ_{rcv} values at different potentials from individual cells. For all panels, $n \geq 3$.

The kinetics of entry into, and recovery from, fast inactivation were also moderately affected by mutating these nine residues (Table I; Fig. 2, B and D). These modest effects of mutations contrast with the dramatic effects observed for homologous residues in potassium channels. This could be the consequence of changing a single residue in the sodium channel, rather than four residues, one in each subunit, in potassium channels.

Perturbation of Channel Gating by Extracellular MTSES Modification and Pattern of Accessibility

Modification of all introduced cysteines was evaluated after two washes after a 10-min application of 5 mM MTSES to the extracellular face of the channel protein. Exposure to extracellular MTSES, even at this relatively high concentration, did not significantly affect the biophysical properties of wild-type (WT) channels or of any of the five innermost mutants in D4/S3 (Table I). These five residues reside in the putative inner helix of S3, below the kink. Channel gating was clearly modified by extracellular MTSES for each of the mutants in the putative external helix (L1433C, L1431C, and G1430C), as well as for the one mutant in the putative kink (S1427C). For these MTSES-sensitive mutants, the two biophysical properties that are consistently affected are steady-state inactivation and recovery from inactivation. After modification by MTSES, the h_∞ curves of these mutants exhibit a hyperpolarized shift, except for L1433C whose h_∞ curve shifted in the depolarized direction. Recovery from inactivation is accelerated only at depolarized potentials for MTSES-modified L1433C and G1430C, but is severely affected for modified L1431C and S1427C. With modified L1431C, the recovery curve shows a ~30-mV hyperpolarized shift and the

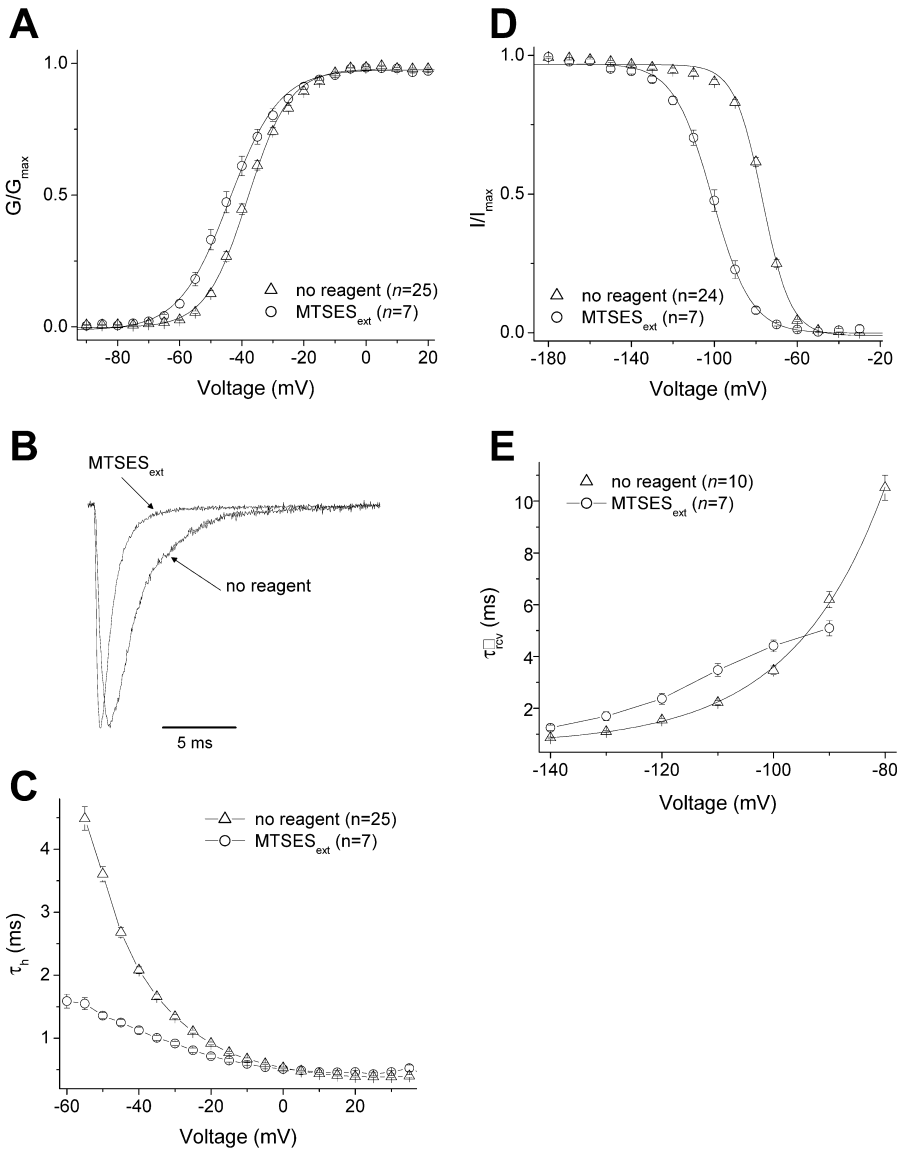

FIGURE 4. Effects of external MTSES on the gating properties of S1427C. Protocols are described in Fig. 2. (A) Voltage-activation relations. (B) Scaled currents were activated by a depolarization from −140 to −40 mV. (C) Fast inactivation. (D) Steady-state inactivation. (E) Recovery from fast inactivation. For the "no reagent" condition, due to variation in the amplitudes of the exponential growth fits from individual cells at the most depolarized potentials, the solid curve shown was not an average of all the fits from individual cells (as in Fig. 3), but was instead a single exponential growth fit to the mean of the τ_{rcv} data from all cells. The two apparent gating charge δ_{rcv}s generated using either method (average of fits vs. fit of averages) were in good agreement (1.51 ± 0.05 [Table I] vs. 1.50, respectively). For the "$MTSES_{ext}$" condition, exponential growth fits could not be performed due to the loss of voltage dependence of τ_{rcv}. For all panels, $n \geq 7$.

slowest rate of recovery (i.e., peak of the recovery curve) is reduced as much as fourfold. With modified S1427C, the voltage dependence of τ_{rcv} is so severely reduced that an exponential growth fit cannot be performed (see below).

The other two biophysical properties that are also affected by MTSES modification in some of these MTSES-sensitive mutants are the kinetics of fast inactivation (τ_h) and the G-V relationship. MTSES modification has little effect on τ_h in L1431C, increases τ_h in L1433C, decreases τ_h in S1427C, and causes a crossover at −45 mV with G1430C (faster inactivation at potentials more hyperpolarized, and slower inactivation at potentials more depolarized, than −45 mV). MTSES treatment causes a small hyperpolarizing shift in G-V curves of both G1430C and S1427C. Together, our data indicate that all four substituted cysteines in the D4/S3 external helix and kink are accessible to extracellular MTSES, whereas there is no evidence that extracellular native cysteines elsewhere in the channel or that the five substituted cysteines in the D4/S3 internal helix are accessible to this reagent. The effects of modification suggest that D4/S3 plays a role, either direct or allosteric, in both activation and inactivation gating.

We will focus our attention on two cysteine mutants, L1433C (the outermost accessible cysteine) and S1427C (the innermost accessible cysteine). Figs. 3 and 4 show the effects of MTSES modification on these two mutants. In L1433C, MTSES modification of L1433C has no effect on the peak G-V relationship (Fig. 3 A), but slows inactivation (Fig. 3, B and C), shifts steady-state inactivation in the depolarized direction (Fig. 3 D), and accelerates recovery from inactivation (Fig. 3 E). Overall, therefore, MTSES modification of L1433C destabilizes inactivated states of the channel. In contrast to L1433C, S1427C modification slightly shifts acti-

TABLE II

Effects of Various Extracellular MTS Reagents on the Gating of Three Cysteine Mutants

	G-V			Inactivation		Steady-state inactivation		
	$V_{0.5}$	δ	*n*	$\tau_{h,\ -40\ mV}$	*n*	$V_{0.5}$	δ	*n*
	mV			*ms*		*mV*		
L1433C	−41.2 ± 0.6	4.10 ± 0.09	14	1.69 ± 0.08	14	−78.0 ± 0.7	4.09 ± 0.11	13
$MTSES_{ext}$	−41.8 ± 0.8	4.15 ± 0.15	8	3.85 ± 0.11[b]	8	−69.4 ± 1.2[b]	3.26 ± 0.06[b]	8
$MTSET_{ext}$	−43.8 ± 0.5[b]	4.04 ± 0.26	5	4.47 ± 0.16[b]	5	−72.1 ± 1.6[a]	3.24 ± 0.07[b]	3
S1427C	−38.2 ± 0.6	3.72 ± 0.04	25	2.08 ± 0.05	25	−76.8 ± 0.5	3.75 ± 0.09	25
$MTSES_{ext}$	−44.0 ± 1.3[b]	3.11 ± 0.09[b]	7	1.13 ± 0.05[b]	7	−100.9 ± 1.5[b]	2.70 ± 0.07[b]	7
$MTSET_{ext}$	−38.0 ± 3.6	2.69 ± 0.22[a]	3	1.52 ± 0.09[b]	5	−92.3 ± 0.6[b]	3.20 ± 0.13[b]	5
$BPMTS_{ext}$	−39.4 ± 1.6	3.15 ± 0.09[b]	4	1.11 ± 0.06[b]	5	−104.0 ± 1.8[b]	1.97 ± 0.06[b]	5
D1420N/S1427C	−35.1 ± 0.5	3.78 ± 0.08	20	2.58 ± 0.07	25	−81.1 ± 0.6	3.52 ± 0.04	24
$MTSES_{ext}$	−41.6 ± 1.4[b]	3.72 ± 0.20	6	1.57 ± 0.08[b]	6	−97.4 ± 0.6[b]	2.45 ± 0.05[b]	7
$MTSET_{ext}$	−37.4 ± 1.3	2.78 ± 0.06[b]	9	2.30 ± 0.13	11	−94.4 ± 0.8[b]	2.64 ± 0.08[b]	11

Not apparent from this table is the small but significant perturbation of fast inactivation in D1420N/S1427C by MTSET, which decreased τ_h at hyperpolarized voltages (e.g., −50 mV) and increased τ_h at depolarized voltages (e.g., 30 mV). Thus, in these three selected mutants, all extracellular MTS reagents appeared to affect both fast inactivation and steady state inactivation. Data are presented as mean ± SEM (*n*).

[a]$P < 0.05$.

[b]$P < 0.01$.

vation in the hyperpolarized direction (Fig. 4 A), accelerates inactivation (Fig. 4, B and C), shifts steady-state inactivation in the hyperpolarized direction (Fig. 4 D), and reduces the voltage dependence of recovery from inactivation (Fig. 4 E). Thus, MTSES modification of S1427C tends to stabilize inactivated states.

Voltage Dependence of Reactivity of L1433C and S1427C

Depolarization moves the three outermost basic residues of the voltage sensor D4/S4 into an external hydrophilic crevice (Yang and Horn, 1995; Yang et al., 1996, 1997). Our present data indicate that the external helix and kink of D4/S3 are also accessible to hydrophilic cysteine reagents. We ask here whether membrane potential affects these accessibilities in D4/S3. Since D4/S3 is a negatively charged transmembrane segment, in contrast to the positively charged voltage sensor D4/S4, we might expect that the direction of voltage dependence for D4/S3 would be opposite to that of D4/S4. Therefore, depolarization might decrease the reactivities of the four accessible cysteines in D4/S3.

Membrane potential (*V*) can affect the rate of MTS modification primarily in two ways in voltage-dependent channels. It affects the conformation of the channel protein, which in turn could alter the reactivity of the cysteine. It can also affect the interaction of a charged reagent with the cysteine by changing the electrostatic potential Ψ_V near that cysteine (Stauffer and Karlin, 1994; Yang et al., 1997; Pascual and Karlin, 1998; Wilson et al., 2000; Elinder et al., 2001). The reactivity of a target cysteine depends on several factors, including its ionization state, its location with respect to the face of the protein on which the hydrophilic cysteine reagent is presented, and steric hindrance in the activated complex between the cysteine thiolate and the reagent. The electrostatic potential Ψ_V is the sum of two components, an intrinsic electrostatic potential ($\Psi_{i,V}$) that depends on the protein conformation, and an extrinsic electrostatic potential, which is the fraction of *V* in the vicinity of the target cysteine (Yang et al., 1997; Pascual and Karlin, 1998).

We use Karlin's ratio-of-ratio method to untangle these two components of Ψ_V (see MATERIALS AND METHODS). This approach allows us to ask three questions for each cysteine examined. First, how does membrane potential affect the reactivity of the cysteine? The answer provides clues to voltage-dependent changes in accessibility, and therefore movement. Second, what is the magnitude and sign of Ψ_V? This information provides clues to the dielectric environment and the presence of charged groups near the cysteine. Third, what fraction of the electric field (δ_{cys}) does the introduced cysteine experience? Large values of δ_{cys} suggest that the cysteine resides in a deep, narrow crevice (see below and DISCUSSION). To answer these three questions, we measured the voltage-dependent modification rates of L1433C and S1427C, the outermost and innermost accessible substituted cysteines, respectively, using the oppositely charge cysteine reagents, MTSET and MTSES. MTSET had no effect on WT channels (unpublished data).

Similar to MTSES, MTSET slows the inactivation of L1433C and shifts its steady-state inactivation in a depolarized direction (Table II). To explore the voltage dependence of L1433C reactivity, we measured rates of

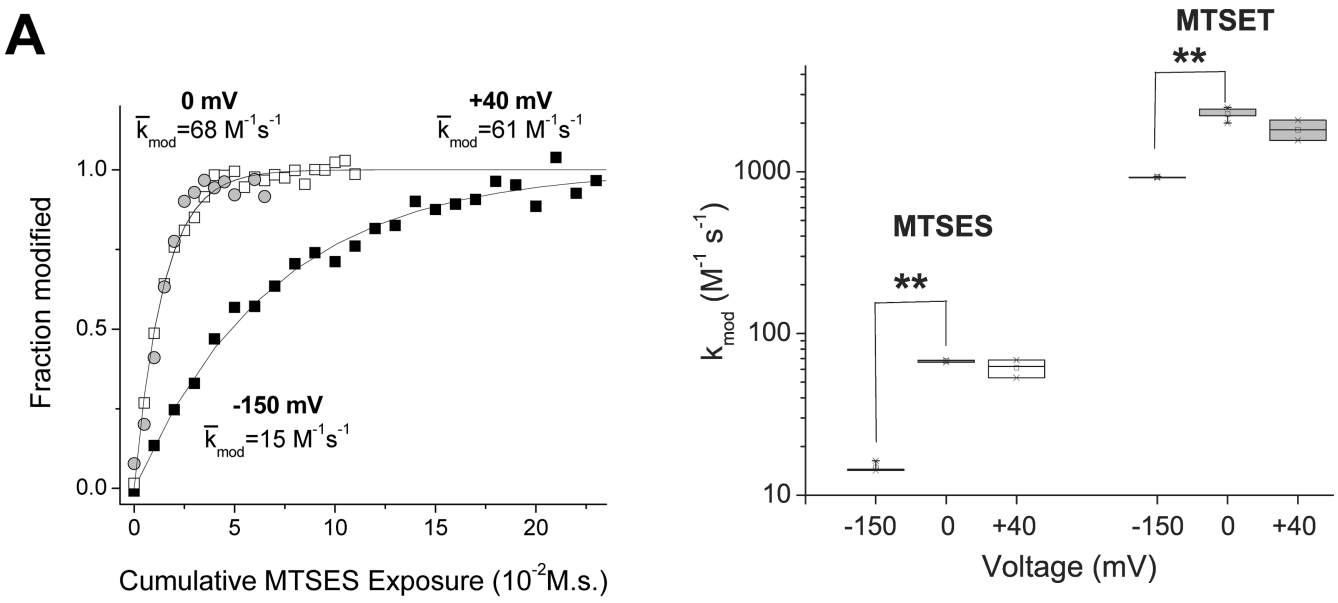

FIGURE 6. Voltage dependence of L1433C modification with MTS reagents. Box plots for k_{mod} (n = 3–5). **P < 0.01.

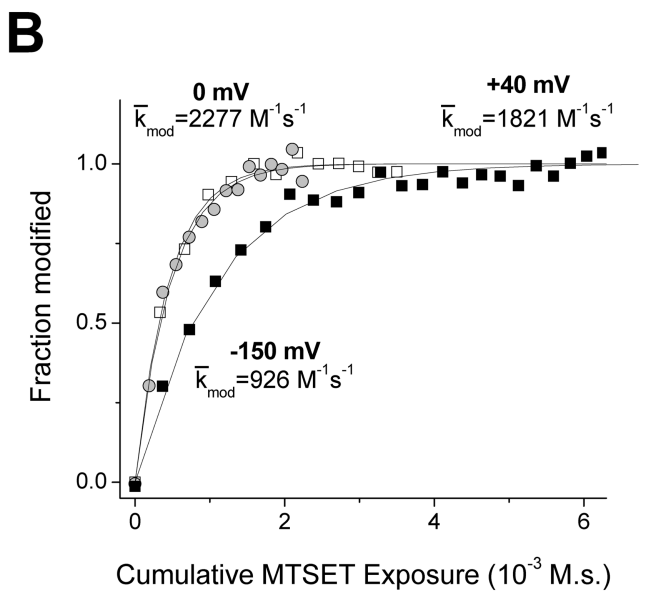

FIGURE 5. Normalized time course of L1433C modification by MTSES (A) and MTSET (B). Modification rates at -150 mV (closed squares) and 0 mV (open squares) and 40 mV (gray circles) were measured by tracking the MTS deceleration of inactivation. Data from representative individual cells were fit with single exponential relaxations, as shown. The k_{mod} values shown for each voltage are mean values of all cells examined at that voltage.

modification by MTSES and MTSET, using a protocol that highlights the slowing of inactivation by these reagents (see MATERIALS AND METHODS). The transfected cells were exposed to reagents under voltage clamp at −150, 0, or 40 mV, using a rapid-exchange perfusion system (see MATERIALS AND METHODS). An inactivating sodium current was then induced at a test pulse of −30 mV, the potential at which both MTS reagents maximally slow inactivation of L1433C (Fig. 3 C). Test pulse currents were always measured in the absence of reagent. Isochronal measurements of current increase tracked the modification, producing estimates of the second order rate constant k_{mod}.

Fig. 5 shows the normalized time course of L1433C modification for MTSES (A) and MTSET (B), using data from representative cells. The data from each cell were fit by a single exponential relaxation to provide an estimate of k_{mod} for each modification voltage, V. Each fitted dataset is labeled with the mean values of k_{mod} for all cells examined at that value of V. For each reagent, k_{mod} increases between −150 and 0 mV, but does not change in response to further depolarization. This conclusion is also demonstrated in the box plot in Fig. 6. The voltage-dependent increase of k_{mod} for both reagents is inconsistent with an effect of voltage solely on Ψ_V. Rather, it indicates a voltage-dependent increase in L1433C reactivity upon depolarization. This change of k_{mod} occurs only over the voltage range where we observe steady-state effects of membrane potential on channel gating (Fig. 3).

A rather different picture emerges for the deeper residue S1427C, based on comparable experiments. Modification of S1427C causes a leftward shift of steady-state inactivation (Fig. 4 D). We used this effect to track modification by measuring the reduction of peak current after a 100-ms prepulse to −90 mV, a voltage which approximately maximizes the magnitude of the reduction. Fig. 7 shows normalized modification curves at three voltages, −150, 0, and 50 mV. As observed for L1433C, k_{mod} for both cysteine reagents increases for a depolarization from −150 to 0 mV, indicating an in-

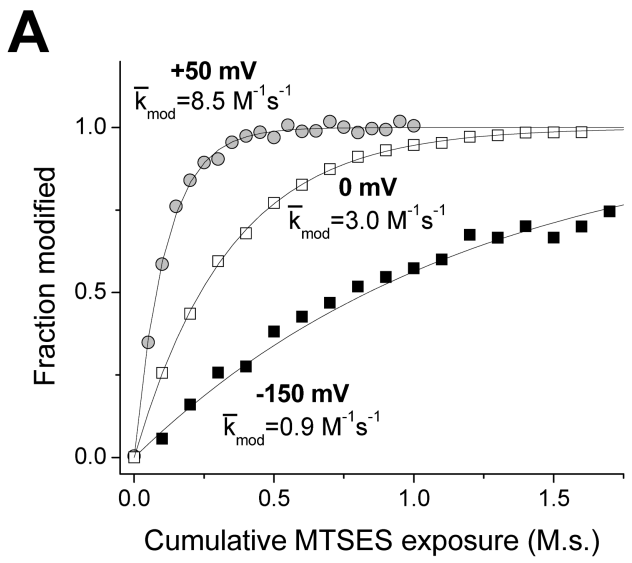

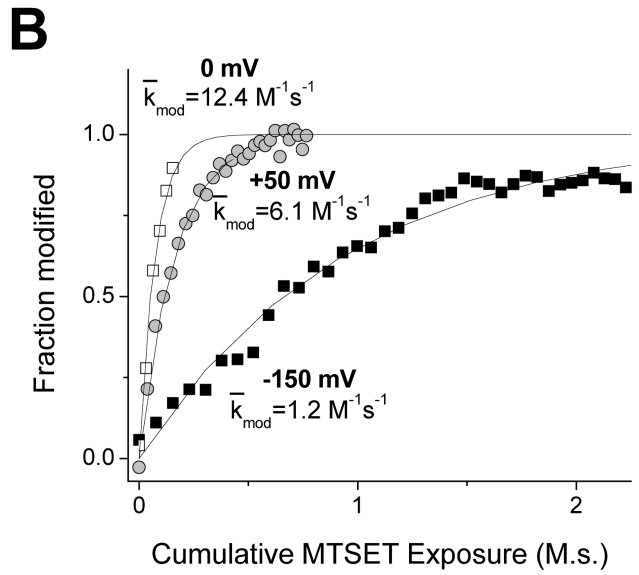

FIGURE 7. Normalized time course of S1427C modification by MTSES (A) and MTSET (B). Modification rates at −150 mV (closed squares) and 0 mV (open squares) and 50 mV (gray circles) were measured by tracking the MTS hyperpolarized shift of steady-state inactivation. Data from representative cells were fit with single exponential relaxations, as shown. The k_{mod} values shown for each voltage are mean values of all cells examined at that voltage.

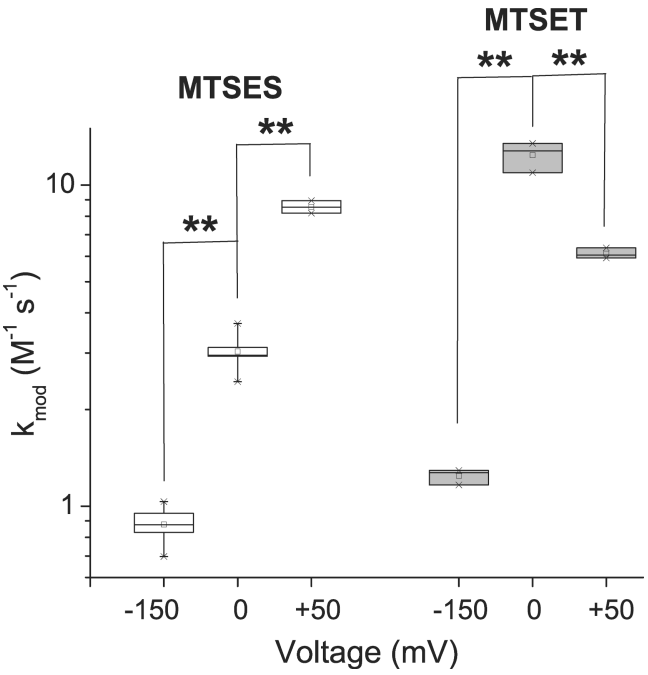

FIGURE 8. Voltage dependence of S1427C modification with MTS reagents. Box plots for k_{mod} (n = 3–5). **P < 0.01.

crease in the reactivity of this cysteine. Further depolarization has different effects, however, for MTSES versus MTSET modification of S1427C. For MTSES a 50-mV depolarization from 0 mV causes a 2.8-fold increase of k_{mod}, but a twofold decrease for MTSET (Figs. 7 and 8). This is exactly the direction of effect expected if S1427C is in the membrane electric field at depolarized voltages, because depolarization would tend to attract the anionic reagent MTSES while repelling the cationic MTSET. Although the effect of depolarization from 0 to 50 mV on k_{mod} is opposite for the two reagents, the magnitude of the effect is not significantly different (2.81 ± 0.44 vs. 2.03 ± 0.23, P = 0.11, z-test). This result supports an important assumption, namely that the different effects of V on the k_{mod} values for these two reagents in this voltage range can be accounted for entirely by their difference in charge, without steric factors playing a significant role. This result supports the use of these reagents as probes of the electrostatic potentials near S1427C, even though the modification rates are very low (<20 $M^{-1}s^{-1}$).

If we assume that the channel undergoes its full range of voltage-dependent conformational changes at voltages negative to 0 mV (Fig. 4), we can use data obtained at V ≥ 0 mV to estimate the fractional distance δ_{cys} of S1427C within the electric field (Eq. 3). For these experiments, δ_{cys} was 0.44 ± 0.05.

We were not able to estimate δ_{cys} at negative potentials because voltage-dependent conformational changes saturate only at extremely hyperpolarized potentials in this sodium channel (e.g., see Yang et al., 1996). Furthermore, we cannot safely extrapolate the estimates of δ_{cys} at depolarized voltages down to −150 mV because of the unknown effects of membrane potential on protein conformation near a crevice. For example, voltage-dependent narrowing of an aqueous crevice would tend to decrease its dielectric constant

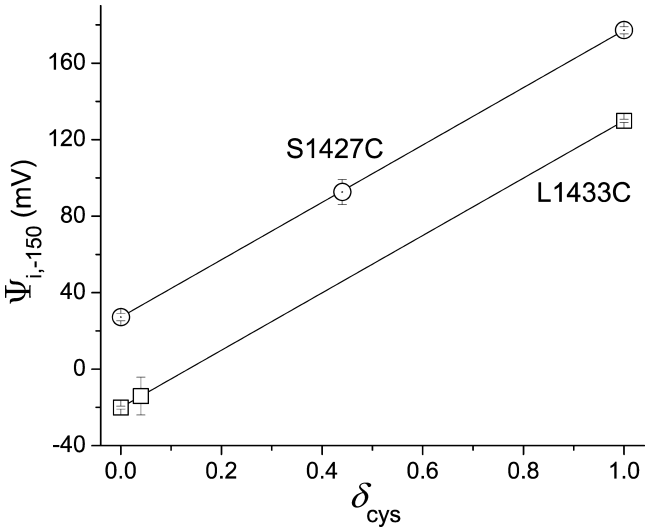

FIGURE 9. Effect of δ_{cys} on $\Psi_{i,-150}$. Modification rates were used to calculate ρ_V, initially at $V = 0$ mV to determine $\Psi_{i,0}$ (Eq. 2). δ_{cys} was estimated from the ratio of ρ_0/ρ_V for positive values of V (Eq. 3). $\Psi_{i,-150}$ was calculated from measured values of ρ_{-150} and Eq. 1, using three different values of δ_{cys}: 0, 1, and the value of δ_{cys} estimated at $V = 0$ mV (plotted symbols for each mutant). For L1433C and S1427C, the estimates of δ_{cys} at 0 mV were 0.04 ± 0.07 and 0.44 ± 0.05, respectively. The theoretical lines show the predicted effect of δ_{cys}, ranging from 0 to 1, on $\Psi_{i,-150}$. Standard errors were determined by propagation of errors (Bevington, 1969). The larger standard errors of $\Psi_{i,-150}$ for intermediate values of δ_{cys} are a consequence of the propagation of errors in estimates of δ_{cys} and the magnitude of V (−150 mV).

(Sansom et al., 1997). This is expected to change the shape of the electric field in a way that would increase δ_{cys} (Islas and Sigworth, 2001).

The modification data for both L1433C and S1427C allow us to estimate an intrinsic electrostatic potential $\Psi_{i,V}$ near these cysteines (see MATERIALS AND METHODS). At positive membrane potentials $\Psi_{i,V}$ is −12.4 ± 1.1 mV for L1433C and 13.9 ± 2.3 mV for S1427C. Therefore, the sign of $\Psi_{i,V}$ is opposite for the two mutants. If we assume that δ_{cys} is the same at −150 mV as it is at 0 mV (see above), then $\Psi_{i,-150}$ = −14.1 ± 9.9 mV for L1433C and 92.6 ± 6.5 mV for S1427C. However, these calculated values of $\Psi_{i,-150}$ are quite sensitive to the assumed values of δ_{cys} (Fig. 9). The moderate decrease in the magnitude of $\Psi_{i,V}$ near L1433C during a depolarization is not significant ($P > 0.05$). However, the magnitude of $\Psi_{i,V}$ decreases significantly near S1427C in response to a depolarization. The increase in reactivity and decrease in magnitude of $\Psi_{i,V}$ suggest that depolarization widens an extracellular crevice in contact with the high impact face of D4/S3, increasing the ability of mobile ions to screen local electrostatic potentials, especially near the relatively inaccessible cysteine in the mutant S1427C.

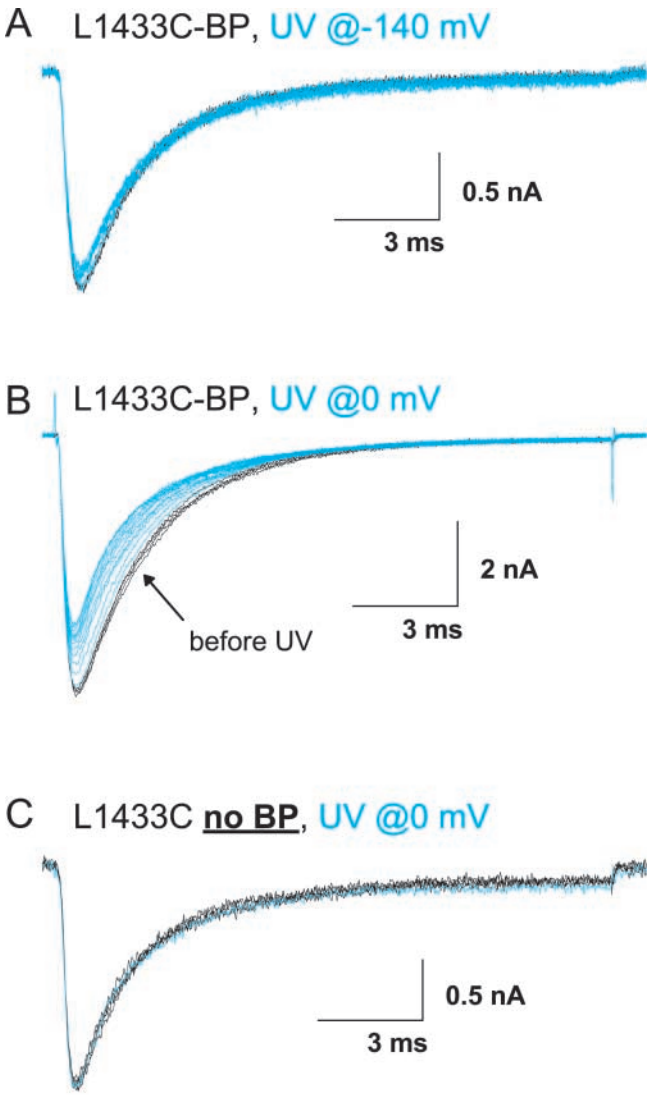

FIGURE 10. Photocross-linking L1433C. Cells in A and B were labeled with BPMTS. Black traces are controls before exposure to UV light. Blue traces were recorded after 2-s exposures to UV light applied either at −140 mV (A) or 0 mV (B and C). See MATERIALS AND METHODS for details.

Immobilization of D4/S3

Immobilization by photocross-linking is an alternative approach, besides changes in cysteine accessibility, to show that regions of ion channels undergo voltage-dependent movement (Horn et al., 2000; Ding and Horn, 2001). The procedure involves testing whether cross-linking an introduced cysteine to neighboring regions of the protein produces measurable effects on the sodium currents. If so, the data support the idea that changes in membrane potential cause movement near the labeled cysteines. Therefore, to explore whether voltage-dependent movement occurs near the external end of D4/S3, we labeled the four accessible cysteine mutants described above with extracellular BPMTS, a

TABLE III

Effect of UV on BPMTS-labeled Cysteine Mutants

	Voltage	Percentage reduction	Parameter	*n*
	mV			
L1433C-BP	−140	6.4 ± 1.2	peak	5
	0	19.5 ± 2.8	peak	4
L1431C-BP	−140	5.8 ± 3.4	τ_h	4
	0	29.7 ± 1.7	τ_h	3
G1430C-BP	−140	14.3 ± 2.4	peak	4
	0	20.0 ± 2.1	peak	4
S1427C-BP	−140	0.1 ± 1.4	peak	3
	0	14.1 ± 1.0	peak	3

Reductions of either peak sodium current or τ_h at −20 mV caused by 22 s irradiation at the indicated membrane potential.

bifunctional photocross-linking cysteine reagent, and observed the consequences of UV irradiation.

Fig. 10, A and B, show the effects of irradiating L1433C after labeling with BPMTS (denoted L1433C-BP). The black traces show 3–4 control currents in response to depolarizations to −20 mV before the first exposure to UV. The subsequent test pulses were preceded by 2-s irradiations at either −140 or 0 mV. When irradiating at 0 mV, the cells were subsequently held at −150 mV for 6.4 s to allow full recovery from inactivation before presenting the test depolarization. Most notably, UV caused a reduction of peak current, especially when presented at 0 mV (Fig. 10 B; Table III). This indicates that the insertion of the benzophenone adduct is more efficient at the depolarized voltage (Ding and Horn, 2001). As in our previous studies with BPMTS-labeled channels, we do not know the insertion target, although it is likely to be a part of the channel within ~10 Å of the S3 segment. The effects of irradiation were not due to nonspecific effects of UV, as shown by the data for an unlabeled cell irradiated at 0 mV (Fig. 10 C). The specificity of UV effects under these experimental conditions was observed for all the D4/S3 mutants (unpublished data). Furthermore, WT sodium channels treated by BPMTS are insensitive to UV irradiation at these intensities (Horn et al., 2000).

The other three accessible mutants were tested using identical protocols after BPMTS labeling, with representative examples shown in Fig. 11 and analysis in Table III. The most notable effect of UV on L1431C-BP was a speeding of inactivation at −20 mV. The effects of UV on G1430C-BP were more complicated, including a decrease in peak current and a slowing of inactivation. For both of these mutants, the insertion efficiency was greater when UV was applied at 0 mV than at −140 mV, as we observed for L1433C-BP (Fig. 10). The least dra-

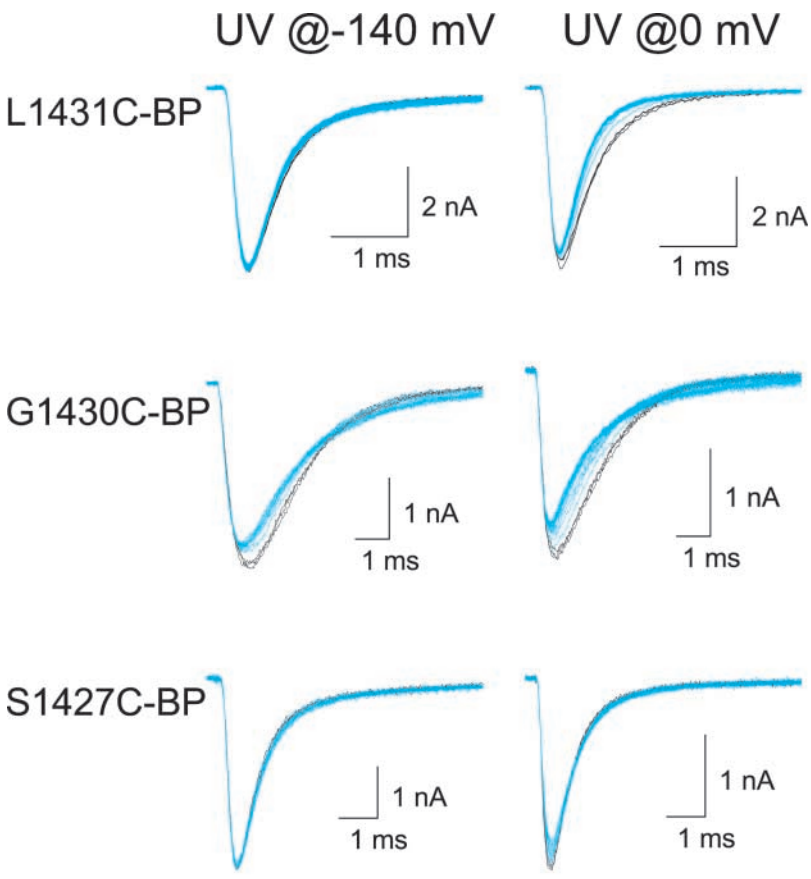

FIGURE 11. Photocross-linking L1431C-BP, G1430C-BP, and S1427C-BP. UV irradiation of BPMTS-labeled cells, as in Fig. 10.

matic effect of UV irradiation, a <20% reduction in peak current, was seen for the deepest accessible mutant, S1427C. This was not due to the inability of the bulky BPMTS reagent to reach S1427C, because we measured clear biophysical consequences of the BPMTS labeling alone (Table II). However, under our experimental conditions we are not certain that all of the channels were labeled.

In summary, photocross-linking experiments show that changes of membrane potential produce movement in the vicinity of D4/S3, consistent with changes in cysteine reactivity.

DISCUSSION

Voltage-dependent gating requires conformational flexibility, a prerequisite for the response to changes of membrane potential. Although some voltage-dependent movements of ion channel proteins may be rather subtle (Sigg et al., 1999), others appear to involve larger rearrangements of the tertiary or quaternary structure. The two best examples of these larger movements (>1 Å) are the translocation of charge by the S4 segment and the opening and closing of gates. A variety of methods have been applied to characterize these movements (see references and discussion in Yellen, 1998; Perozo et al., 1999; Bezanilla, 2000; Horn et al., 2000; Horn, 2000). In this study, we used two approaches to examine movement near an S3 segment of the sodium channel, cysteine scanning and immobilization by a photoactivatable cross-linker. Both approaches provide evidence for voltage-dependent movement in a region of sodium channels heretofore unexamined.

Hydrophilic Crevices

Cysteine-scanning studies have shown that hydrophilic crevices almost completely surround the positively charged S4 segments of voltage-gated potassium and sodium channels (Bezanilla, 2000; Horn, 2000). The apparent role of these crevices is twofold, to obviate the energetic cost of burying positively charged S4 residues in a hydrophobic environment and to allow relatively modest movements to transfer several S4 charges across the membrane electric field (Yang et al., 1996). The presence of crevices around other transmembrane segments has not been examined as extensively, other than the central crevice comprising the permeation pathway. Moreover, the presence of an extensive network of water-filled crevices around uncharged transmembrane segments might itself pose an energetic problem by exposing the side chains of hydrophobic residues to water. However, to prevent direct interaction between positively charged S4 segments and lipid, it is reasonable to suppose that S4 segments are partially surrounded by all the other transmembrane segments (Horn, 2000). This implies that all other transmembrane segments contribute to the lining of the aqueous crevices surrounding the S4 segment.

Our principal tool for characterizing the crevices and vestibules around transmembrane segments is the reaction of introduced cysteines with hydrophilic methanethiosulfonate reagents (Karlin and Akabas, 1998). This approach has its limitations, some of which we would like to mention. First, the reagents that we use, MTSET and MTSES, have significant dimensions (~6 Å × 10 Å) compared with those of sodium channels (~65 Å × 100 Å; Sato et al., 2001) and with the thickness of the bilayer (~35–45 Å). This has consequences. For example, the reactive MTS lies at the opposite end of the molecule from the charged trimethylammonium or sulfonate moieties, meaning that the cysteine thiol may experience a different local electrostatic environment than that reported by the charged ends of the molecules (Yang et al., 1997). Furthermore, to estimate electrostatic potentials we assume that these two reagents are indistinguishable, except for charge and inherent reactivity with free thiols. However, the low modification rates, especially for S1427C, make steric differences between the reagents a concern. Some of this concern is alleviated, however, by the relatively simple and consistent patterns we observe for modification rates at different membrane potentials (Figs. 5–8). Most notably, the effects of depolarizations beyond 0 mV can be explained entirely by the opposite charges of MTSES and MTSET, and the position of the cysteines within the electric field. Another concern is that we use the implicit assumption that at any voltage or conformational state we are probing a fixed structure; however, the covalent modification may occur only during transient exposures of the cysteine thiol. Relatively large-scale fluctuations of backbone atoms have been shown to accompany the entry of small molecules into protein interiors (Feher et al., 1996). Finally, cysteine substitution itself may alter the conformation of a preexisting crevice, or even create a crevice in a formerly hydrophobically closed region. With these caveats in mind, we have used MTSET and MTSES to probe the crevices and vestibules around transmembrane segments.

Our results show that the extracellular end of the high impact face of an S3 segment of $Na_V1.4$ sodium channels is accessible to hydrophilic cysteine reagents. Based solely on primary sequence, the accessible residues extend ~40% along the length of this S3 segment, reaching down to S1427C. This part of the S3 segment has been proposed to form an amphipathic α-helix partially interfacing with the extracellular aqueous solution (Li-Smerin and Swartz, 2001). Fig. 1 A shows an alignment of sodium and potassium channel S3 seg-

ments. Interestingly, two of our accessible residues (L1431C and L1433C) are equivalent to *drk1* S3 residues (I273 and L275) believed to participate in binding of hydrophilic Hanatoxin (Li-Smerin and Swartz, 2000, 2001). Mutation of *drk1* residue L275 (equivalent to our L1433) to lysine also has a large effect on voltage-dependent gating (Li-Smerin and Swartz, 2001), suggesting that this residue is involved in protein–protein interactions, befitting its designation as a high impact residue. L275 could experience both an aqueous and a buried environment if changes in membrane potential altered its environment. Because Hanatoxin binding is favored at hyperpolarized voltages (Swartz and MacKinnon, 1997a), residue L275 is predicted to have decreased aqueous accessibility at depolarized voltages. This is the opposite of our results for the homologous residue L1433C, which shows increased reactivity to MTS reagents at depolarized voltages. This discrepancy may be a consequence of structural differences between D4/S3 of a sodium channel and the *drk1* S3 segment; alternatively, the large effects of mutating I273 and L275 on toxin binding may be allosteric, rather than an indication that these residues directly contact the toxin. Nevertheless, the results from both types of channels are consistent with voltage-dependent movement at the extracellular end of S3 segments.

What is the nature of the extracellular crevice adjacent to D4/S3? First, it extends at least as deeply as residue S1427C. Second, it must be at least 6 Å wide to accommodate MTSET. Third, the crevice appears to narrow as it dips into the hydrophobic core of the channel protein. This conclusion is based on two results, the relative rates of modification for L1433C and S1427C, and the estimates of electrical distance δ_{cys} for these two residues. S1427C is 1-to-2 orders of magnitude less reactive to MTS reagents, as if it were in a more restricted environment. Furthermore, δ_{cys} is $\sim$0 for L1433C and 44% through the electric field for S1427C. Some of this difference might be explained by the physical locations of these two residues, with L1433C being closer to the extracellular end of D4/S3 than S1427C. However, the large value of δ_{cys} for S1427C is inconsistent with a wide hydrophilic crevice, because if an aqueous crevice reaches only partway through a transmembrane protein, the transmembrane electric field will tend to fall primarily across the lower-dielectric protein, rather than across the hydrophilic crevice (Islas and Sigworth, 2001). Only a narrow crevice with a correspondingly low dielectric constant (Sansom et al., 1997) would be capable of supporting significant values of δ_{cys}.

Our examination of the extracellular crevice near D4/S4 suggests the presence of a negative intrinsic electrostatic potential $\Psi_{i,V}$ that increases in magnitude at greater depths into the core of the protein (Yang et al., 1997), exactly as expected if the narrowing walls focus the potential generated by a negatively charged residue at the bottom of the crevice (Getzoff et al., 1983; Klapper et al., 1986). By contrast, in D4/S3 $\Psi_{i,V}$ has a different sign for the superficial residue L1433C than for the deeper residue S1427C, suggesting that these two residues experience very different local environments.

Could the S3 and S4 segments share the same crevice, i.e., do these two transmembrane segments line the same extracellular space? This idea is supported by the fact that Hanatoxin appears to interact with the extracellular ends of both S3 and S4 segments of *drk1* potassium channels (Swartz and MacKinnon, 1997b). Furthermore, negative charges in the S3 segment are proposed to interact electrostatically with positive charges of S4 (Papazian et al., 1995). In D4 of $Na_V1.4$, however, there are two noticeable differences in the properties of the extracellular regions adjacent to S3 and S4 segments. First, the deepest accessible residue we have found in D4/S4 is not within the electric field when it is exposed extracellularly (Yang et al., 1997). Second, although S4 residues experience negative values of $\Psi_{i,V}$, one of the two residues we examined here, S1427C, experiences a positive $\Psi_{i,V}$. Neither of these differences discounts the possibility that the high impact face of D4/S3 and D4/S4 share the same crevice. The large value of δ_{cys} and the low rates of modification for S1427C suggest, however, that it lies in a deeper and less accessible region than any of the S4 residues we studied. The positive $\Psi_{i,V}$ in the vicinity of S1427C further suggests that it might be close to the S4 segment, where it would be exposed to the electrostatic potentials generated by basic S4 residues. We will explore further implications of a shared S3-S4 crevice below.

Voltage-dependent Movement Near D4/S3

Depolarization from −150 to 0 mV increases the reactivity of both L1433C and S1427C to both cysteine reagents. Although other options are possible, the simplest explanation for these increases in reactivities is that depolarization increases the aqueous accessibility of the high impact face of the extracellular helix of D4/S3. This increased reactivity might be caused by D4/S3 moving outward. Moreover, the decreased magnitude of $\Psi_{i,V}$ caused by depolarization of S1427C suggests that depolarization enhances the screening by mobile ions of the extracellular solution. This would be the consequence of a widening of the extracellular crevice facing S1427C.

The magnitudes of the voltage dependence of modification rates for both L1433C and S1427C are small (2–10-fold over a range of 150 mV) compared, for example, with the pronounced state dependence of accessibilities of cysteines in the D4/S4 segment (Yang and Horn, 1995; Yang et al., 1996) or the S6 segment of

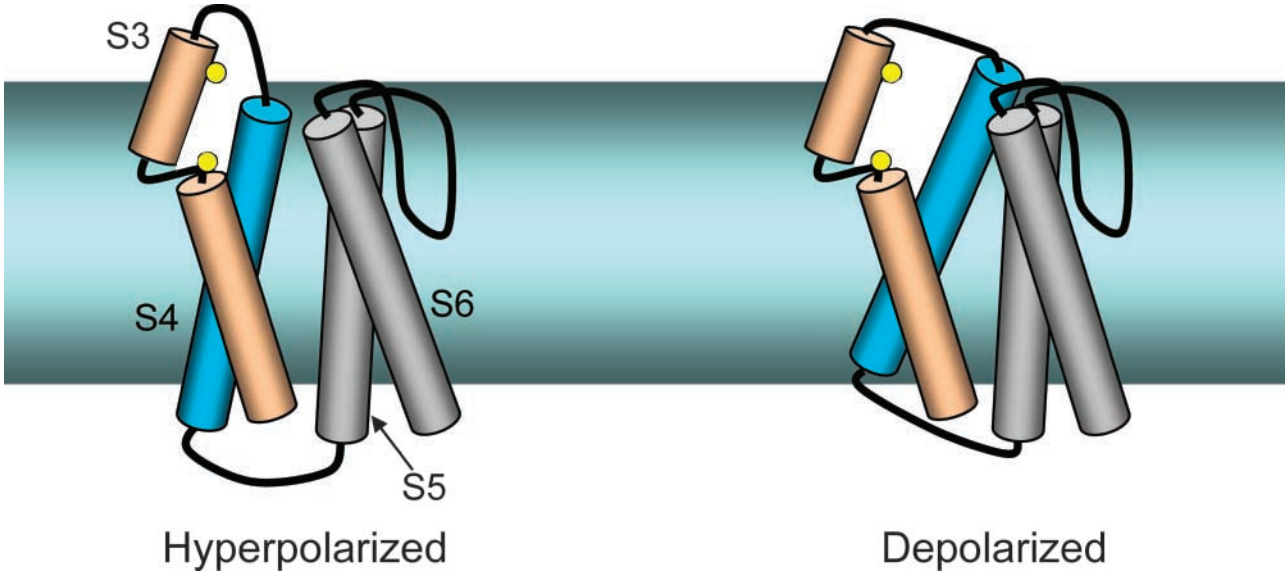

FIGURE 12. Crevice-widening model. Transmembrane segments S4–S6 are shown as cylinders, and S3 is shown as two cylinders separated by a kink (Li-Smerin and Swartz, 2001). The permeation pathway is to the right of the S6 segment. The S1 and S2 segments are not shown. The yellow balls represent cysteine substituted for either L1433C in the outer helix or S1427C in the kink. A crevice (exaggerated for clarity) is shown between the outer ends of S3 and S4. Depolarization causes an outward movement of S4 and a tilt toward the pore, widening the crevice between S3 and S4. S3 is shown as fixed, although it is likely that it moves in response to changes in the conformations of the transmembrane segments that abut it.

potassium channels (Liu et al., 1997). However, the voltage dependence is larger than that observed for a cysteine substituted near the extracellular end of the S2 segment of the *Shaker* potassium channel (Tiwari-Woodruff et al., 2000). It would be of interest to know if the changes in D4/S3 reactivity track the movement of the S4 segment of D4. That is, how much of the voltage-dependent changes in k_{mod} can be accounted for by S4 movement? Unfortunately, the small changes in cysteine reactivity between −150 and 0 mV preclude a detailed examination of the voltage dependence. Nevertheless, our data show that L1433C and S1427C are always partially accessible from the extracellular surface of the channel, and that voltage-dependent conformational changes modestly alter the environment of the extracellular helix of this S3 segment. Experiments using UV irradiation of BPMTS-labeled cysteines also indicate the presence of voltage-dependent movement near D4/S3.

Our results do not support a significant role for D4/S3 as a voltage sensor. First, the direction of the changes in reactivity of substituted cysteines is the opposite of that expected for a negatively charged voltage sensor, namely an inward translational movement upon depolarization, unless the inward movement of the conserved D1420 through the electric field moves the extracellular end of D4/S3 into a wider region of an extracellular crevice. Second, neutralization of D1420 to either cysteine or asparagine has only moderate effects on gating (Tables I and II). Finally, we have measured cysteine modification of the double mutant D1420N/S1427C in preliminary experiments. Although neutralizing D1420 alters the reactivity of the introduced cysteine, a qualitatively similar result emerges when the membrane potential is changed. Namely, we observe an increase in reactivity upon depolarization. With MTSET k_{mod} increased from 1.00 ± 0.07 to 2.67 ± 0.14 $M^{-1}s^{-1}$ (n = 4, 3), and with MTSES k_{mod} increased from 0.32 ± 0.02 to 2.22 ± 0.07 $M^{-1}s^{-1}$ (n = 3), for a depolarization from −150 to 0 mV. The absence of a direct role for D4/S3 as a voltage sensor agrees with previous data examining the homologous S3 residue (D316) in *Shaker* potassium channels (Seoh et al., 1996).

If D4/S3 is not a voltage sensor, how does membrane potential alter the accessibilities of its residues to hydrophilic reagents? One possibility is that movement of neighboring transmembrane segments, especially the D4/S4 voltage sensor, produces a compensatory movement of the D4/S3 segment in a way that enhances the exposure of its high impact face. S4 might, for example, carry the S3 segment outward as it translocates its own charged residues outward through the electric field. The cartoon in Fig. 12 shows another possibility that does not involve a movement of S3 itself, using a kinked model of the S3 segment (Li-Smerin and Swartz, 2001). Depolarization might cause an outward translocation of the S4 segment including a movement toward the S5 and S6 segments, as proposed for the *Shaker* potassium channel (Loots and Isacoff, 2000; Elinder et al., 2001). This movement would widen a

crevice (exaggerated for clarity) between the extracellular ends of the S3 and S4 segments, enhancing accessibility to the two residues we have examined (shown as yellow balls). A displacement of S3 away from S4 during a depolarization was also proposed for *Shaker* potassium channels (Gonzalez et al., 2001). The negative $\Psi_{i,V}$ near L1433C in this view comes from the S3-S4 linker, whereas the positive $\Psi_{i,V}$ near S1427C is due to basic residues of the S4 segment. Our model does not show the locations of the S1 or S2 segments, or how their positions might change, relative to S3, during a depolarization. Although one face of S2 segments appear to face lipid (Monks et al., 1999; Li-Smerin et al., 2000), the S2 and S3 segments also share an extracellular crevice in a potassium channel, where they both contribute to a Mg^{2+} binding site (Silverman et al., 2000). The increased efficiency of photocross-linking at depolarized voltages suggests that another transmembrane segment or extracellular loop is closer to the S3 segment at depolarized voltages. If our crevice-widening model holds, the insertion target is unlikely to be the S4 segment but could, for example, be the S2 segment.

The model in Fig. 12 calls into question the role of the S3-S4 linker in gating. Recent studies show that shortening this linker affects voltage-dependent gating (Gonzalez et al., 2000, 2001), perhaps by restricting S4 movement. An extreme example of linker length is seen in a bacterial sodium channel that has only two residues in its S3-S4 linker (Ren et al., 2001). In this case, movement of the S3 segment might be obligatory when the S4 segment moves.

Finally, we return to the question of the possible roles of water-filled crevices around transmembrane segments that are predominantly hydrophobic. As suggested above, these crevices may provide important access pathways for functional modulation by soluble extracellular factors, such as inorganic ions and other small molecules. Critical extracellular crevices may also have been exploited by evolving toxins. Another possibility is that the conformational flexibility underlying voltage-dependent gating may require a network of hydrophilic crevices to counteract the tight adherence between mutually hydrophobic transmembrane segments. From this vantage point voltage-gated ion channels are more like transmembrane transporters such as lac permease than the simple bacterial potassium channel KcsA. Not only is lac permease riddled with aqueous crevices, as shown by extensive cysteine scanning experiments (Venkatesan et al., 2000a,b,c), but its hydrogen/deuterium exchange rate is much higher than that of KcsA (le Coutre and Kaback, 2000). The two-transmembrane segment KcsA channel may not require a high degree of conformational flexibility for its function. Although such flexibility may be essential for the function of voltage-gated ion channels, it might create obstacles to the determination of high-resolution structures.

We thank Mike O'Leary and Manuel Covarrubias for insightful comments on the manuscript, and Keith Scarfo for technical support.

Supported by National Institutes of Health grant AR41691 (to R. Horn).

Submitted: 30 May 2002
Revised: 15 July 2002
Accepted: 22 July 2002

REFERENCES

Bevington, P.R. 1969. Data Reduction and Error Analysis for the Physical Sciences. McGraw-Hill, New York. pp. 56–65.

Bezanilla, F. 2000. The voltage sensor in voltage dependent ion channels. *Physiol. Rev.* 80:555–592.

Cannon, S.C., L.J. Hayward, J. Beech, and R.H. Brown, Jr. 1995. Sodium channel inactivation is impaired in equine hyperkalemic periodic paralysis. *J. Neurophys.* 73:1892–1899.

Cha, A., and F. Bezanilla. 1997. Characterizing voltage-dependent conformational changes in the *Shaker* K^+ channel with fluorescence. *Neuron.* 19:1127–1140.

Ding, S., and R. Horn. 2001. Slow photo-cross-linking kinetics of benzophenone-labeled voltage sensors of ion channels. *Biochemistry.* 40:10707–10716.

Elinder, F., R. Männikkö, and H.P. Larsson. 2001. S4 charges move close to residues in the pore domain during activation in a K channel. *J. Gen. Physiol.* 118:1–10.

Feher, V.A., E.P. Baldwin, and F.W. Dahlquist. 1996. Access of ligands to cavities within the core of a protein is rapid. *Nat. Struct. Biol.* 3:516–521.

Getzoff, E.D., J.A. Tainer, P.K. Weiner, P.A. Kollman, J. Richardson, and D.C. Richardson. 1983. Electrostatic recognition between superoxide and copper, zinc superoxide dismutase. *Nature.* 306: 287–290.

Gonzalez, C., E. Rosenman, F. Bezanilla, O. Alvarez, and R. Latorre. 2000. Modulation of the *Shaker* K^+ channel gating kinetics by the S3-S4 linker. *J. Gen. Physiol.* 115:193–207.

Gonzalez, C., E. Rosenman, F. Bezanilla, O. Alvarez, and R. Latorre. 2001. Periodic perturbations in *Shaker* K^+ channel gating kinetics by deletions in the S3-S4 linker. *Proc. Natl. Acad. Sci. USA.* 98: 9617–9623.

Hong, K.H., and C. Miller. 2000. The lipid-protein interface of a *Shaker* K^+ channel. *J. Gen. Physiol.* 115:51–58.

Horn, R. 1998. Explorations of voltage-dependent conformational changes using cysteine scanning. *Methods Enzymol.* 293:145–155.

Horn, R. 2000. Conversation between voltage sensors and gates of ion channels. *Biochemistry.* 39:15653–15658.

Horn, R., S. Ding, and H.J. Gruber. 2000. Immobilizing the moving parts of voltage-gated ion channels. *J. Gen. Physiol.* 116:461–475.

Islas, L.D., and F.J. Sigworth. 2001. Electrostatics and the gating pore of *Shaker* potassium channels. *J. Gen. Physiol.* 117:69–89.

Ji, S., A.L. George, Jr., R. Horn, and R.L. Barchi. 1996. Paramyotonia congenita mutations reveal different roles for segments S3 and S4 of domain D4 in hSkM1 sodium channel gating. *J. Gen. Physiol.* 107:183–194.

Jurman, M.E., L.M. Boland, Y. Liu, and G. Yellen. 1994. Visual identification of individual transfected cells for electrophysiology using antibody-coated beads. *Biotechniques.* 17:876–881.

Karlin, A., and M.H. Akabas. 1998. Substituted-cysteine accessibility method. *Methods Enzymol.* 293:123–145.

Keynes, R.D., and F. Elinder. 1999. The screw-helical voltage gating

of ion channels. *Proc. R Soc. Lond. B Biol. Sci.* 266:843–852.

Klapper, I., R. Hagstrom, R. Fine, K. Sharp, and B. Honig. 1986. Focusing of electric fields in the active site of Cu-Zn superoxide dismutase: effects of ionic strength and amino acid modification. *Proteins.* 1:47–59.

le Coutre, J., and H.R. Kaback. 2000. Structure-function relationships of integral membrane proteins: Membrane transporters vs channels. *Biopolymers.* 55:297–307.

Li-Smerin, Y., D.H. Hackos, and K.J. Swartz. 2000. α-Helical structural elements within the voltage-sensing domains of a K^+ channel. *J. Gen. Physiol.* 115:33–49.

Li-Smerin, Y., and K.J. Swartz. 2000. Localization and molecular determinants of the hanatoxin receptors on the voltage-sensing domains of a K^+ channel. *J. Gen. Physiol.* 115:673–684.

Li-Smerin, Y., and K.J. Swartz. 2001. Helical structure of the COOH terminus of S3 and its contribution to the gating modifier toxin receptor in voltage-gated ion channels. *J. Gen. Physiol.* 117:205–217.

Liu, Y., M. Holmgren, M.E. Jurman, and G. Yellen. 1997. Gated access to the pore of a voltage-dependent K^+ channel. *Neuron.* 19: 175–184.

Loots, E., and E.Y. Isacoff. 2000. Molecular coupling of S4 to a K^+ channel's slow inactivation gate. *J. Gen. Physiol.* 116:623–635.

Margolskee, R.F., B. McHendry-Rinde, and R. Horn. 1993. Panning transfected cells for electrophysiological studies. *Biotechniques.* 15:906–911.

Mitrovic, N., A.L. George, Jr., and R. Horn. 1998. Independent versus coupled inactivation in sodium channels - Role of the domain 2 S4 segment. *J. Gen. Physiol.* 111:451–462.

Mitrovic, N., A.L. George, Jr., and R. Horn. 2000. Role of domain 4 in sodium channel slow inactivation. *J. Gen. Physiol.* 115:707–718.

Monks, S.A., D.J. Needleman, and C. Miller. 1999. Helical structure and packing orientation of the S2 segment in the *Shaker* K^+ channel. *J. Gen. Physiol.* 113:415–423.

O'Leary, M.E., L.-Q. Chen, R.G. Kallen, and R. Horn. 1995. A molecular link between activation and inactivation of sodium channels. *J. Gen. Physiol.* 106:641–658.

Papazian, D.M., X.M. Shao, S.-A. Seoh, A.F. Mock, Y. Huang, and D.H. Wainstock. 1995. Electrostatic interactions of S4 voltage sensor in *Shaker* K^+ channel. *Neuron.* 14:1293–1301.

Pascual, J.M., and A. Karlin. 1998. State-dependent accessibility and electrostatic potential in the channel of the acetylcholine receptor - Inferences from rates of reaction of thiosulfonates with substituted cysteines in the M2 segment of the α subunit. *J. Gen. Physiol.* 111:717–739.

Perozo, E., D.M. Cortes, and L.G. Cuello. 1999. Structural rearrangements underlying K^+-channel activation gating. *Science.* 285:73–78.

Planells-Cases, R., A.V. Ferrer-Montiel, C.D. Patten, and M. Montal. 1995. Mutation of conserved negatively charged residues in the S2 and S3 transmembrane segments of a mammalian K^+ channel selectively modulates channel gating. *Proc. Natl. Acad. Sci. USA.* 92:9422–9426.

Ptacek, L.J., L. Gouw, H. Kwiecinski, P. McManis, J.R. Mendell, R.J. Barohn, A.L. George, Jr., R.L. Barchi, M. Robertson, and M.F. Leppert. 1993. Sodium channel mutations in paramyotonia congenita and hyperkalemic periodic paralysis. *Ann. Neurol.* 33:300–307.

Ren, D.J., B. Navarro, H.X. Xu, L.X. Yue, Q. Shi, and D.E. Clapham. 2001. A prokaryotic voltage-gated sodium channel. *Science.* 294:2372–2375.

Sansom, M.S., G.R. Smith, C. Adcock, and P.C. Biggin. 1997. The dielectric properties of water within model transbilayer pores. *Biophys. J.* 73:2404–2415.

Sato, C., Y. Ueno, K. Asai, K. Takahashi, M. Sato, A. Engel, and Y. Fujiyoshi. 2001. The voltage-sensitive sodium channel is a bell-shaped molecule with several cavities. *Nature.* 409:1047–1051.

Seoh, S.A., D. Sigg, D.M. Papazian, and F. Bezanilla. 1996. Voltage-sensing residues in the S2 and S4 segments of the *Shaker* K^+ channel. *Neuron.* 16:1159–1167.

Sigg, D., H. Qian, and F. Bezanilla. 1999. Kramers' diffusion theory applied to gating kinetics of voltage-dependent ion channels. *Biophys. J.* 76:782–803.

Sigworth, F.J. 1994. Voltage gating of ion channels. *Q. Rev. Biophys.* 27:1–40.

Silverman, W.R., C.-Y. Tang, A.F. Mock, K.-B. Huh, and D.M. Papazian. 2000. Mg^{2+} modulates voltage-dependent activation in ether-à-go-go potassium channels by binding between transmembrane segments S2 and S3. *J. Gen. Physiol.* 116:663–677.

Stauffer, D.A., and A. Karlin. 1994. Electrostatic potential of the acetylcholine binding sites in the nicotinic receptor probed by reactions of binding-site cysteines with charged methanethiosulfonates. *Biochemistry.* 33:6840–6849.

Swartz, K.J., and R. MacKinnon. 1997a. Hanatoxin modifies the gating of a voltage-dependent K^+ channel through multiple binding sites. *Neuron.* 18:665–673.

Swartz, K.J., and R. MacKinnon. 1997b. Mapping the receptor rite for Hanatoxin, a gating modifier of voltage-dependent K^+ channels. *Neuron.* 18:675–682.

Tiwari-Woodruff, S.K., M.C.A. Lin, C.T. Schulteis, and D.M. Papazian. 2000. Voltage-dependent structural interactions in the *Shaker* K^+ channel. *J. Gen. Physiol.* 115:123–138.

Tiwari-Woodruff, S.K., C.T. Schulteis, A.F. Mock, and D.M. Papazian. 1997. Electrostatic interactions between transmembrane segments mediate folding of *Shaker* K^+ channel subunits. *Biophys. J.* 72:1489–1500.

Vedantham, V., and S.C. Cannon. 1998. Slow inactivation does not affect movement of the fast inactivation gate in voltage-gated Na^+ channels. *J. Gen. Physiol.* 111:83–93.

Venkatesan, P., Y. Hu, and H.R. Kaback. 2000a. Site-directed sulfhydryl labeling of the lactose permease of *Escherichia coli*: helix X. *Biochemistry.* 39:10656–10661.

Venkatesan, P., I. Kwaw, Y. Hu, and H.R. Kaback. 2000b. Site-directed sulfhydryl labeling of the lactose permease of *Escherichia coli*: helix VII. *Biochemistry.* 39:10641–10648.

Venkatesan, P., Z. Liu, Y. Hu, and H.R. Kaback. 2000c. Site-directed sulfhydryl labeling of the lactose permease of *Escherichia coli*: N-ethylmaleimide-sensitive face of helix II. *Biochemistry.* 39: 10649–10655.

Wilson, G.G., J.M. Pascual, N. Brooijmans, D. Murray, and A. Karlin. 2000. The intrinsic electrostatic potential and the intermediate ring of charge in the acetylcholine receptor channel. *J. Gen. Physiol.* 115:93–106.

Yang, N., A.L. George, and R. Horn. 1997. Probing the outer vestibule of a sodium channel voltage sensor. *Biophys. J.* 73:2260–2268.

Yang, N., A.L. George, Jr., and R. Horn. 1996. Molecular basis of charge movement in voltage-gated sodium channels. *Neuron.* 16: 113–122.

Yang, N., and R. Horn. 1995. Evidence for voltage-dependent S4 movement in sodium channels. *Neuron.* 15:213–218.

Yang, N., S. Ji, M. Zhou, L.J. Ptácek, R.L. Barchi, R. Horn, and A.L. George, Jr. 1994. Sodium channel mutations in paramyotonia congenita exhibit similar biophysical phenotypes in vitro. *Proc. Natl. Acad. Sci. USA.* 91:12785–12789.

Yellen, G. 1998. The moving parts of voltage-gated ion channels. *Q. Rev. Biophys.* 31:239–295.